The Molecular Code for Hemoglobin Allostery Revealed by Linking the Thermodynamics and Kinetics of Quaternary Structural Change. 2. Cooperative Free Energies of $(\alpha_{FeCO}\beta_{Fe})_2$ and $(\alpha_{Fe}\beta_{FeCO})_2$ T-State Tetramers[†]

Robert A. Goldbeck,*,[‡] Raymond M. Esquerra,[§] David S. Kliger,[‡] Jo M. Holt,[||] and Gary K. Ackers[||]

Department of Chemistry and Biochemistry, University of California, Santa Cruz, California 95064, Department of Chemistry and Biochemistry, San Francisco State University, San Francisco, California 94132, and Department of Biochemistry and Molecular Biophysics, Washington University School of Medicine, St. Louis, Missouri 63110

ABSTRACT: Ligand photodissociation experiments are used to measure the prephotolysis equilibria between doubly liganded R and T quaternary conformers of the symmetric Fe−Co HbCO hybrids, $(\alpha_{FeCO}\beta_{Co})_2$ and $(\alpha_{Co}\beta_{FeCO})_2$. The free energies obtained from these data are used to calculate the cooperative free energies of the $(\alpha_{FeCO}\beta_{Fe})_2$ and $(\alpha_{Fe}\beta_{FeCO})_2$ intermediate CO-ligation states of normal hemoglobin in the T conformation, quantities important to the evaluation of current models of cooperativity. The symmetry rule model, incorporating sequential cooperativity of T-state ligand binding within an $\alpha\beta$ dimer in addition to the traditional two-state cooperativity of the tetramer, predicts a larger free energy penalty for disturbing both dimers in a doubly liganded T tetramer than would be expected in the two-state model as currently formulated. (Cooperative energy penalties are simply proportional to the number of tetramer-bound ligands in the traditional two-state model.) The value found here for the energies of doubly liganded T microstates in which both dimers are perturbed, 7.9 ± 0.3 kcal/mol, is consistent with the symmetry rule model but significantly higher than that expected (5−6 kcal/mol) in the two-state model of cooperativity.

A novel kinetic model describing the ligand rebinding and quaternary structural relaxation reactions of HbCO after ligand photodissociation is presented in our companion article (*1*). This model provides a framework that promises to systematize and unify the description of the allosteric and ligand binding reactions of hemoglobin by relating the free energies of activation to the free energies of reaction via linear free energy relations (LFERs).[1] It has been known for some time that the kinetics of the bimolecular ligand binding and the R→T quaternary transition reactions of hemoglobin can each be described by LFERs (*2, 3*). The microstate linear free energy relation (MLFER) model combines the LFER approach with recent advances in the thermodynamic characterization of allostery (*4*) to simultaneously apply LFERs to both the quaternary structural relaxation and ligand binding reaction kinetics on the microscopic level of all twenty R and T quaternary conformation/ligation microstates of the hemoglobin tetramer.

Cooperative free energies, $^{ij}\Delta G_c$, for most of the twenty ^{ij}R and ^{ij}T microstates in HbCO can be obtained for input into the model directly from thermodynamic measurements (*5*) or reasonable extrapolations therefrom (*1*). However, an important subset of $^{ij}\Delta G_c$ values, those for the T-conformer microstates containing a single ligand on each dimer ([22], [23], and [24] ligation in the Ackers [*ij*] indexing convention), was not available from equilibrium data. We thus turned to ligand photodissociation kinetic studies of the symmetrical iron−cobalt metal hybrids of HbCO, $(\alpha_{FeCO}\beta_{Co})_2$ (species **23**) and $(\alpha_{Co}\beta_{FeCO})_2$ (species **24**), to determine the respective energies $^{23}\Delta G_c(T)$ and $^{24}\Delta G_c(T)$.

The cobaltous porphyrins in **23** and **24** do not bind CO (*6, 7*), allowing their complexes to serve as equilibrium models for the [23] and [24] ligation states of fully ferrous hemoglobin. The latter are difficult to observe at equilibrium because cooperative ligand binding tends to suppress the populations of intermediate ligation states in favor of the end states, T_0 (^{01}T) and R_4 (^{41}R). Substituting both the α- or β-chain irons with cobalt permits equilibrium measurements on these otherwise ephemeral intermediate ligation states, while preserving the essential features of cooperativity (see ref *5* and references therein). Given that the stabilities of doubly liganded hemoglobins are generally expected to lie near the switch point between the R and T quaternary conformers, solutions of **23** and **24** can be expected to contain significant populations of both forms. The free energies $^{23}\Delta G_c(T)^{Co/FeCO}$ and $^{24}\Delta G_c(T)^{Co/FeCO}$ can then be obtained from measurements of T/R equilibria in the respective hybrid. These equilibria are measured in the present work with a

---

method first developed by Marden et al. (*8*) that uses the distinctly different kinetics of the R and T forms after ligand photodissociation to assess their relative populations in the prephotolysis sample. (In contrast, direct thermodynamic measurements of these equilibria are difficult because their effect on the cooperative free energies will be small compared to the noise in such measurements, ± 0.3 kcal/mol.) It is then possible to "translate" the hybrid cooperative free energies to the values desired for normal hemoglobin, $^{23}\Delta G_c(T)^{Fe/FeCO}$ and $^{24}\Delta G_c(T)^{Fe/FeCO}$, by applying known transformation rules (*5*).

Measuring these microstate energies is important in evaluating the ability of specific models of hemoglobin cooperativity to describe the effect of ligation on conformational free energy throughout the range of ligation states available to the T quaternary conformer. Previous evidence for the symmetry rule model, obtained from thermodynamic measurements of microstate cooperative free energies in hemoglobins stripped of allosteric effectors, rested on the observation that all ligation species with at least one ligand bound to each dimer are dominantly in the R conformation. This is in contrast to the traditional two-state model, in which the relative stability of R and T conformers depends only on the number of ligands bound to the tetramer (*9*). The structural basis of the symmetry rule is attributed to a lower energy penalty associated with perturbing the structure of one dimer in the T quaternary state, as opposed to perturbing both dimers. A crucial difference between the models is thus the existence or absence of the T_2 free energy gap, $^{2n}\Delta G_c(T) - {}^{21}\Delta G_c(T)$ ($n \neq 1$). This gap was observed to be at least 2.3 kcal/mol in previous thermodynamic measurements of HbCO microstate energies supporting the symmetry model (*5*), whereas it is postulated to be zero in traditional two-state models. Equilibrium measurements on hemoglobin in solution have been limited in assessing this energy gap because one cannot observe the continuing perturbation of T-conformational energies as ligands are added beyond the symmetry "switch point" for the quaternary transition. Such measurement are effectively "leveled" by the greater stability and relative insensitivity to increasing ligation of the R conformers after the ligation switch point is passed. The $^{ij}\Delta G_c$ values for ^{23}T and ^{24}T inferred here from kinetic measurements thus help fill this gap and permit a more direct evaluation of the T_2 $^{ij}\Delta G_c$ gap.

The $^{ij}\Delta G_c$ values calculated from the cobalt hybrid photolysis data allow us to determine the energies of T-conformation microstates, ^{23}T and ^{24}T, that cannot be observed directly in equilibrium experiments on normal hemoglobin. With the energies measured here, 7.9 ± 0.3 kcal/mol for both $^{23}\Delta G_c(T)$ and $^{24}\Delta G_c(T)$, we can now complete with greater confidence the picture of T conformer microstate energies drawn previously from the thermodynamic data. Overall, this picture shows that the dominant perturbation of T conformational energy observed throughout the ligation series occurs when a ligand is added to a previously unliganded dimer, the perturbation free energy accompanying addition of a second ligand to a dimer being two to three times smaller. The principle of relative dimer independence underlying the symmetry rule, the idea that the conformational accommodations of the tetramer to ligation-induced forces within a given quaternary state (R or T) occur relatively independently within each dimer, as

Scheme 1
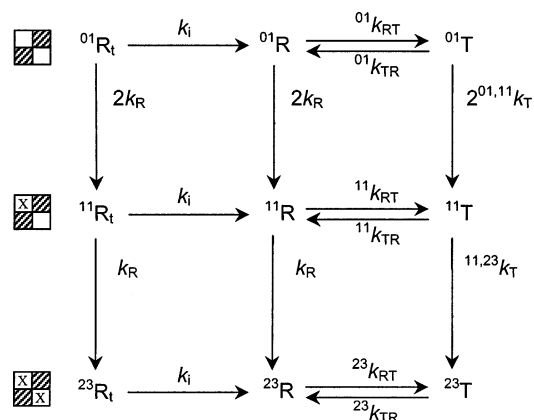
Scheme 2
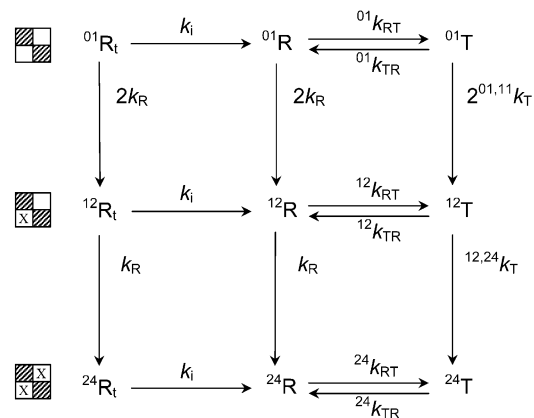
opposed to the relative monomer independence of traditional two-state models (the monomers within each dimer being, after all, much more tightly bound to each other than are the dimers), is thus confirmed by the remarkably close correspondence found here between the thermodynamic and kinetic evidence.

MATERIALS AND METHODS

The cobalt–iron hemoglobin hybrid species **23** and **24** were prepared as described by Huang and Ackers (*5*). Soret region time-resolved absorption spectra were measured after photodissociation of the CO-complexed hybrids (under 1 atm CO) as described in (*1*). The stripped samples (120 μM in heme) had been column-stripped of the physiological allosteric effector DPG. Effector-bound samples were produced from the stripped hybrids by adding 2 mM IHP. All samples were in pH 7.4 buffered solutions containing 0.1 M Tris, 0.1 M NaCl, and 1 mM EDTA, maintained at 20 ± 1 °C.

KINETIC MODELING PROCEDURES

The MLFER modeling procedures used below were based on the model for normal hemoglobin presented in the companion paper (*1*). That model is modified in the present work to account for the effect of heme metal substitution on ligand binding, effector binding, dimer–dimer association, and microstate cooperative free energies. Schemes 1 and 2 present the microscopic rate constants for the kinetics of ligand binding and quaternary structure change after CO photodissociation from the cobalt hybrids **23** and **24**, respectively. The kinetic model for the geminate recombina-

Scheme 3

| Heme Type	$[Fe \cdots CO]_r$	$[Fe \cdots]_r$	$[Fe \cdots CO]_t$	$R_{t,0}$	R_0	T_0	$R_{t,1}$	R_1	T_1	$R_{t,2}$	R_2	T_2	D
R_r	2	2	0	0	0	0	0	0	0	0	0	0	0
R_t	0	0	2	2	0	0	1	0	0	0	0	0	0
R	0	0	0	0	2	0	0	1	0	0	0	0	2
T	0	0	0	0	0	2	0	0	1	0	0	0	0

tion phase of the post-photolysis reactions was identical to that presented in (*1*). That geminate recombination kinetic scheme (per heme basis) was combined with the bimolecular recombination and allosteric kinetics presented in Scheme 1 or 2 (per tetramer basis) of the present work by the use of statistical factors that depend on the number of heme sites available to bind ligands. These factors, calculated using simple combinatorial statistics, describe the distribution of geminately recombined hemes within the tetramers. To illustrate, the reaction step

$$[Fe \cdots CO]_t \xrightarrow{k_6} [Fe \cdots]_t$$
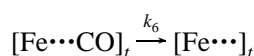
in the (per heme) geminate recombination kinetics was replaced with the two (per tetramer) steps

$$[Fe \cdots CO]_t \xrightarrow{C_0 k_6} R_{t,0} \qquad (1)$$

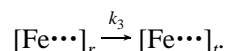$$[Fe \cdots CO]_t \xrightarrow{C_1 k_6} R_{t,1} \qquad (2)$$
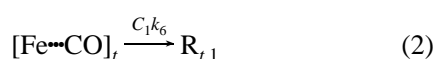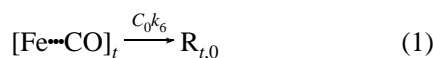
where the statistical factors C_n are given by

$$C_n = n P_n / \sum_{n'=0}^{1} n' P_{n'} \qquad (3)$$

$$P_n = \frac{2!}{(2-n)! \, n!} p^{2-n} (1-p)^n \qquad (4)$$

and p is the net photolysis yield after geminate recombination. A similar replacement was made for

$$[Fe \cdots]_r \xrightarrow{k_3} [Fe \cdots]_t.$$

Cooperative Free Energies of Hybrid Species. The MLFER model uses the free energies of quaternary structure transformation and ligand binding reactions to predict relationships between the activation energies of those reactions for individual R and T conformational microstates. Those energies are calculated in turn from the microstate cooperative free energies. The cooperative free energies of all of the equilibrium cobalt hybrid CO-ligation species have been measured previously (*5*), but the photolysis products of the **23** and **24** hybrids studied in the present work also include several nonequilibrium species whose energies have not been measured. The equilibrium energies used in the present work (wherein all cooperative free energies are referenced to $^{01}\Delta G_c(T)$ of Hb A$_0$ as the zero of energy) are shown in Table 1. Also shown are the energies of the T conformations of the [11] and [12] species for the **23** and **24** hybrids, respectively. Although those energies have not been mea-

Table 1: Microstate Thermodynamic Parameters for **23** and **24** Cobalt−Iron HbCO Hybrids (0.1 M Cl$^-$)^a

Species^b	[ij]	$^{ij}\Delta G_c{}^c$	Equilibrium conformation	$^{ij}K_{RT}{}^d$
23 hybrid				
	[01]	0.3 ± 0.3	T	9×10^4
	[11]	3.4 ± 0.5	T	400
	[23]	6.9 ± 0.3	R	0.2
24 hybrid				
	[01]	2.8 ± 0.3	T	1×10^3
	[12]	5.4 ± 0.5	T	20
	[24]	7.0 ± 0.3	R	0.09

^{a} Free energies are referenced to $^{01}\Delta G_c(T)$ of Hb A$_0$ as zero of energy, in kcal/mole. ^{b} Tetrameric Co/FeCO ligation species. Orientation of α and β subunits are indicated in species **23**[01]. Open squares represent unliganded Fe subunits, X-filled squares represent liganded subunits, and crosshatched squares represent cobalt substitution. ^{c} Energies of unliganded and fully liganded species are from data of Huang and Ackers (*5*). Energies of the partially liganded species [11] and [12] were estimated from equilibrium data using rules described in the text. ^{d} Calculated from $^{ij}\Delta G_c$ values in Figure 9.

sured directly in thermodynamics experiments, in principle they can be estimated (albeit within wide error margins) from the equilibrium data using the following transformation rules for Fe → Co substitution inferred by Huang and Ackers (*5*): (1) replacing iron with cobalt on an α heme increases the $^{ij}\Delta G_c$ by 1.5 kcal/mol, but (2) if the β heme in the same dimer is bound to CO, the energy increase diminishes to 0.4 kcal/mol, and (3) replacing iron with cobalt on the β heme of a dimer already containing an α cobalt increases the energy by an additional 0.4 kcal/mol. In other words, cobalt substitution at an α heme produces the dominant energy perturbation, although coupling to ligand binding within the same dimer can decrease this effect, whereas substitution at a β heme produces a negligible energy perturbation unless it is coupled to α substitution within the same dimer. When these rules were applied to the cooperative free energies of the [11] ligation species, both the Co/FeCO hybrid **11** (5.4 kcal/mol) and Hb$_A$CO (3.3 kcal/mol) produced similar estimates for the energy of the **23**[11] nonequilibrium ligation species, the average estimate being shown in Table 1. A similar procedure using the energies of the ligated **12** cobalt hybrid (6.0 kcal/mol) and the [12] ligation species of normal hemoglobin (3.4 kcal/mol) yielded the consensus estimate

shown for the energy of the hybrid **24**[12] ligation species. However, because of the relatively large uncertainties in these estimates and the sensitivity of the model to their values, they were not used directly in the set of experimentally fixed cooperative energy values from which reaction energies were calculated in the model. Instead, the energies of the **23**[11] and **24**[12] T conformer species were made free parameters to be optimized in the fitting procedure, starting from the estimated energies as initial values, and the optimized values were used to calculate reaction free energies. This left three remaining species for each hybrid whose energies were not available from equilibrium measurements, specifically, the less stable quaternary conformer corresponding to each species in Table 1. As we did for normal hemoglobin in the companion paper, we assumed here that the cooperative free energies of the R conformers are relatively independent of perturbations. We thus set the unknown energies of the R-microstates $^{01}R_{23}$ and $^{11}R_{23}$ of the **23** hybrid equal to the experimental energy of $^{23}R_{23}$, and similarly for the **24** hybrid, we set the energies of $^{01}R_{24}$ and $^{12}R_{24}$ equal to the experimental energy of $^{24}R_{24}$. Finally, the last unknown cooperative free energies, those for the $^{23}T_{23}$ and $^{24}T_{24}$ microstates, were made free parameters in the model. Note that it is from the values of those parameters that we then calculate, using the cobalt perturbation rules described above, the free energies of the ^{23}T and ^{24}T microstates of normal hemoglobin. The energies determined here thus provide important inputs to the MLFER model for normal hemoglobin presented in our companion paper (*1*).

As is the case for normal hemoglobin, the allosteric effector IHP is known to bind more strongly to the deoxy T state than to the liganded R state of cobalt hybrid hemoglobins (*10*). The free energies of effector binding are used in the MLFER model to calculate the T-microstate cooperative free energies in the presence of IHP, starting from experimental energies measured in the absence of IHP. However, quantitative measures of the IHP binding energies do not seem to be available for the hybrids. In the absence of experimental values for the effector binding energies, we made these free parameters in the model, allowing for a CO-ligation dependence of effector binding by separately parametrizing the energies for the zero and doubly ligated T-states and interpolating values for the singly ligated microstates. (These values were referenced to the IHP binding energy of the R states as the zero of energy, the latter energy being assumed to be independent of ligation.)

Microstate Rate Constants for Ligand Binding and Quaternary Transition. The relative allosteric activation energies were then calculated from

$$^{ij}\Delta G^{\ddagger}_{RT} = \alpha_{RT}(^{ij}\Delta G_{RT} - {}^{01}\Delta G_{RT}) + {}^{01}\Delta G^{\ddagger}_{RT} \quad (5)$$

where the value of the linear free energy parameter α_{RT} was taken to be 0.2, the value for normal hemoglobin. This approach fixed the values of the microscopic R→T rate constants $^{ij}k_{RT}$ to within a common factor ($^{01}k_{RT}$), which was optimized as a parameter in the model. Thus,

$$^{ij}k_{RT} = {}^{01}k_{RT} \exp(-\alpha_{RT}(^{ij}\Delta G_{RT} - {}^{01}\Delta G_{RT})/RT) \quad (6)$$

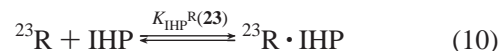where R is the gas constant and T is temperature.

As explained more completely in the companion article (*1*), thermodynamic linkage between the cooperative and ligand binding energies leads to the following relationship between the T and R microstate ligand binding rate constants:
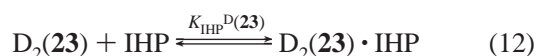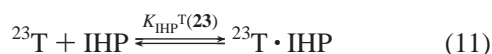
$$^{ij,(i+1)k}k_T =$$
$$k_R \exp(-\alpha_{CO}(^{(i+1)k}\Delta G_c(T) - {}^{ij}\Delta G_c(T))/RT) \quad (7)$$

where (ij) and $((i + 1)k)$ index the reactant and product microstates, respectively. The values of the two free parameters in this relation, k_R and α_{CO}, were determined by optimizing the fit of the model to the data.

Summarizing the MLFER model parametrization for the cobalt hybrids, 10 parameters were optimized simultaneously in the fitting of the model to the data: three geminate time constant parameters, g_1, g_2, and g_3 (*1*); $^{01}k_{RT}$, k_R, and α_{CO}; and four free energies, the latter corresponding to $^{01}\Delta G_{IHP}$, $^{23}\Delta G_{IHP}$, $^{11}\Delta G_c(T)$, and $^{23}\Delta G_c(T)$ in the case of hybrid **23** and $^{01}\Delta G_{IHP}$, $^{24}\Delta G_{IHP}$, $^{12}\Delta G_c(T)$, and $^{24}\Delta G_c(T)$ for hybrid **24**. Also including the additional free parameter, τ_3, independently optimized in a global fit of a 6-exponential decay expression to the data (*1*) means that the model presented here used a total of eleven parameters to describe the full time course of ligand rebinding and structural relaxation in photolyzed cobalt-hybrid-HbCO. The procedures used to optimize the values of these parameters in fitting of the kinetic data are described in ref *1*, the heme spectral-type matrix **M** introduced therein by eq A15 being defined here by Scheme 3 for the hybrids.

Dimer−Tetramer and Effector Binding Equilibria. The model accounted for the multiple equilibria corresponding to the T_2/R_2 equilibrium (eq 8), dissociation of carboxy R tetramers into dimers (eq 9), and the binding of IHP to the R_2, T_2, and dimer species (eqs 10−12) in the prephotolysis sample containing each hybrid. (Photolysis-induced changes in dimerization and effector binding were neglected, as these were expected to occur too slowly to significantly influence hemoglobin allostery on the time scales investigated here.) Free energy values for the dissociation of the R_2 forms of the **23** and **24** hybrids into dimers ($\Delta G_D = -RT \ln(K_D)$) were taken from Huang and Ackers (*5*). As experimental measurements of the free energy of IHP binding to the R_2 species of the cobalt hybrids do not seem to be available, they were estimated here using the rough approximation that the trend observed for normal hemoglobin (*11*), in which the binding energy for the R form (ΔG^R_{IHP}) is about half of that for the deoxy T form ($^{01}\Delta G_{IHP} \equiv \Delta G^T_{IHP} - \Delta G^R_{IHP} \approx \Delta G^T_{IHP}/2$), applies to the cobalt hybrids as well. Finally, the binding energy for the dimer form was estimated from the data of Gray (*12*) to be about 1 kcal/mol less stable than that for the R form ($\Delta G^D_{IHP} \approx \Delta G^R_{IHP} + 1.0$ kcal/mol).

$$^{23}R \underset{}{\overset{L_2(23)}{\rightleftharpoons}} {}^{23}T \quad (8)$$

$$^{23}R \underset{}{\overset{K_D(23)}{\rightleftharpoons}} 2D_2(23) \quad (9)$$

$$^{23}R + IHP \underset{}{\overset{K_{IHP}{}^R(23)}{\rightleftharpoons}} {}^{23}R \cdot IHP \quad (10)$$

$$^{23}T + IHP \xrightleftharpoons{K_{IHP}^{T(\mathbf{23})}} {}^{23}T \cdot IHP \qquad (11)$$

$$D_2(\mathbf{23}) + IHP \xrightleftharpoons{K_{IHP}^{D(\mathbf{23})}} D_2(\mathbf{23}) \cdot IHP \qquad (12)$$

and analogous equations for species **24**. (Note that D$_2$ in the above equations refers to a doubly CO-ligated dimer.)

RESULTS

The time dependent plot of the **23** hybrid Soret band photolysis difference spectrum shown in Figure 1a contains kinetic contributions from both the R and T quaternary forms, the former giving rise to geminate and ~100-μs time-scale diffusive recombination of CO ligand and the latter giving rise to CO recombination on the millisecond time scale. The addition of IHP shifts the prephotolysis equilibrium of quaternary species strongly to the T form for the **23** hybrid, as the amount of geminate recombination and microsecond diffusive recombination are sharply reduced in Figure 1b, leaving millisecond CO-recombination to dominant the kinetics. A similar shifting of the prephotolysis equilibrium toward the T form upon addition of IHP is also evident in the time dependent photolysis spectra of the **24** hybrid (Figure 2) as a decrease in the amplitudes of the geminate and diffusive R-state ligand recombination processes, although the effect is not as dramatic as that seen in Figure 1 for the **23** hybrid.

These effects can be seen more clearly in the SVD component V$_1$, which corresponds to the approximate time course of CO recombination (*1*). V$_1$ decays via geminate recombination to about 70% of its initial value by 1 μs after photolysis and then decays via second-order recombination in two kinetic phases of roughly similar amplitudes corresponding to R-state (~100 μs) and T-state (millisecond) recombinations, respectively, in the stripped **23** hybrid (Figure 3b). This is in contrast to the time course observed in native HbCO (see Figure 5d in ref *1*) in which the amplitude of the T-state recombination is much smaller than that of R. Given that the geminate recombination yield of the T form of the protein is expected to be negligibly small (*8, 13*), the smaller amplitude of the geminate recombination phase in the hybrid vs the native protein (~30 vs 35%) suggests that a significant fraction of the hybrid sample is present as the T form before photolysis. This prephotolysis T population is expected to remain in the T form after photolysis and thus contribute to the larger amplitude of T-state CO recombination that is observed in the hybrid. Addition of IHP to the **23** hybrid reduces the geminate recombination phase of V$_1$ to less than 5% of the total signal and, while distinct phases corresponding to second-order R- and T-state recombination can still be discerned, the former is much smaller in amplitude than the latter (Figure 4b). These observations are consistent with a prephotolysis sample that is dominated by the T quaternary form of the protein in the presence of IHP, as expected from the strongly stabilizing interaction of IHP with the T state. A similar trend is observed in the V$_1$ time course upon addition of effector to the **24** hybrid (Figures 5b and 6b), although again it is not as pronounced as that observed for the **23** hybrid.

A rough estimate of the energy difference between the R$_2$ and T$_2$ microstates was obtained for each hybrid by compar-

FIGURE 1: Time-resolved Soret region absorption spectra of photolyzed Co–Fe hybrid HbCO species **23**. Photolysis difference spectra for hybrid (a) stripped of DPG and (b) plus IHP.

ing the amplitude of its geminate ligand rebinding to that for native HbCO. The latter, being entirely in the R conformer, has the maximum geminate amplitude of the three HbCO porphyrin-metalation forms compared here. The ratio of the geminate rebinding amplitudes for a given hybrid to that for the native then provided an estimate of the prephotolysis fractional population of R state conformers for that hybrid. Using geminate rebinding amplitudes obtained from a phenomenological 6-exponential fit to the kinetic data for the hybrids (Table 2) and native HbCO (see Table 3 in ref *1*) gave values of 0.37, 0.38, and 0.44 for the stripped **23**, **24**, and native amplitudes, respectively. (We assigned the two fastest exponential processes observed in the stripped hybrids to geminate recombination on the basis of the close similarity of the time constants (see Table 2) and decay spectra (Figures 7 and 8) of the hybrids to those for the corresponding geminate processes in native HbCO (*1*). Note in this regard that all of the exponential decay processes observed in the hybrid samples corresponded reasonably well in lifetime, decay spectrum, and thus physical assignment, to the analogous processes in native HbCO, with a small exception in the case of **23** + IHP. In the latter case, only the fastest exponential process corresponded to geminate rebinding. Thus, processes 2–4 in hybrid **23** corresponded to processes 3–5, respectively, in the native protein + IHP, and processes 5 and 6 in the hybrid together correspond to process 6 (T-state rebinding) in the native sample. A similar correspondence in phenomenological rate processes between
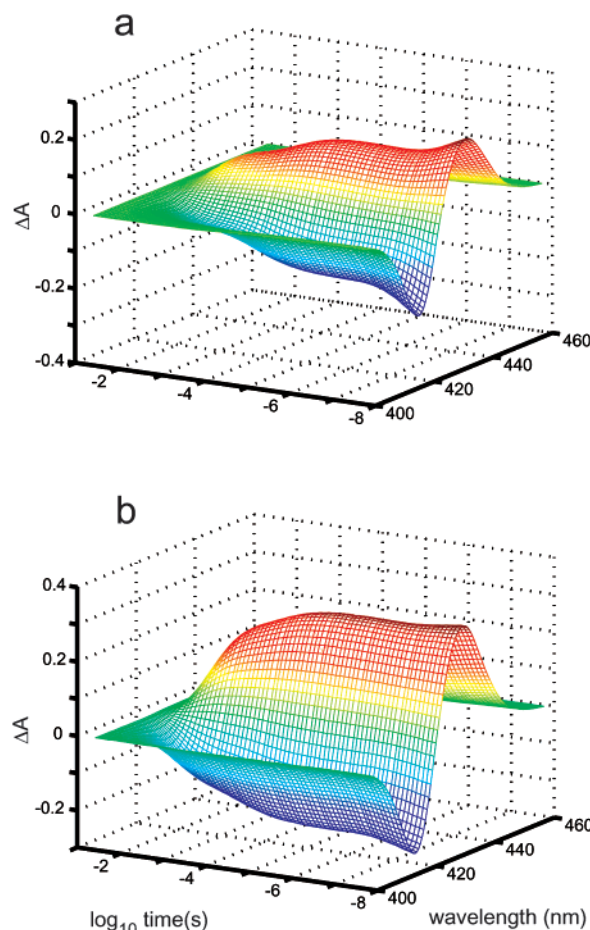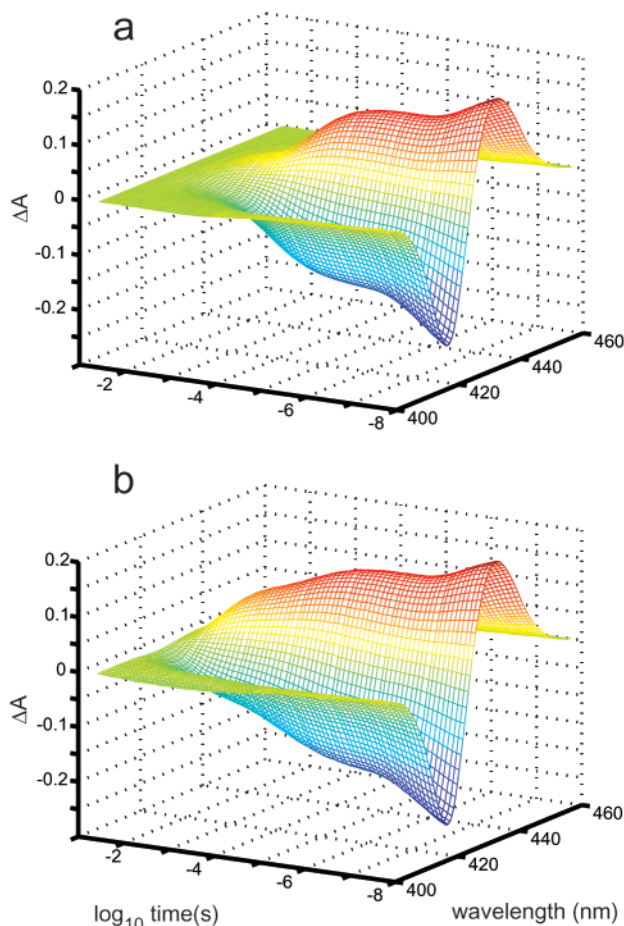
FIGURE 2: Time-resolved Soret region absorption spectra of photolyzed Co−Fe hybrid HbCO species **24**. Photolysis difference spectra for hybrid (a) stripped of DPG and (b) plus IHP.
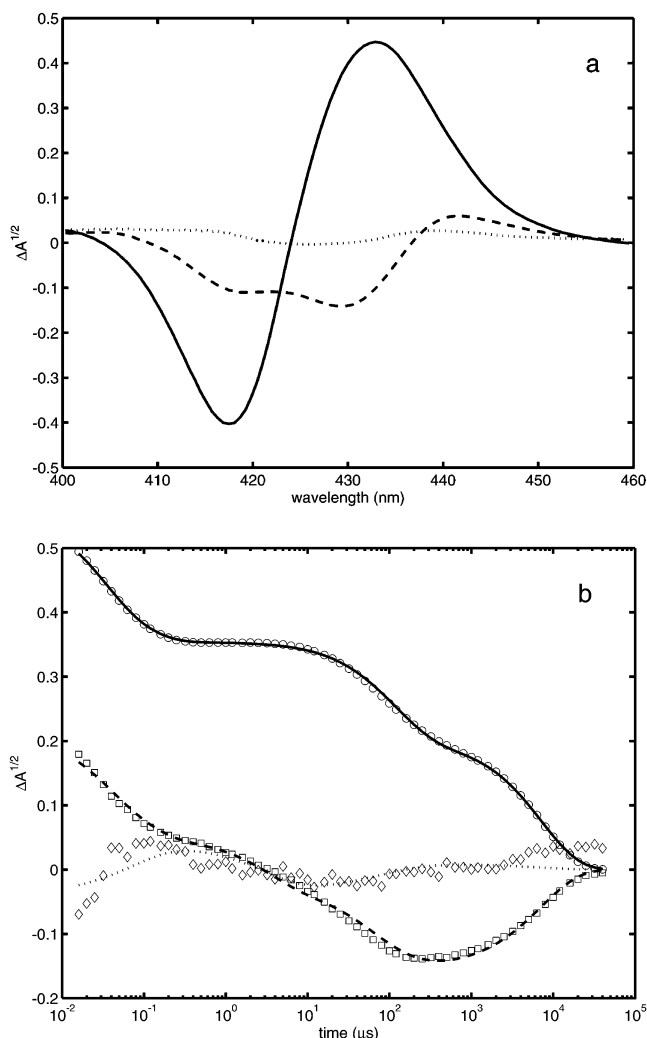

FIGURE 3: The first three SVD components of photolysis data for stripped hybrid HbCO **23**. (a) Basis spectra, $S_1^{1/2}U_1$ (−), $S_2^{1/2}U_2$ (- - -), and $S_3^{1/2}U_3$ (•••). (b) Temporal amplitudes are shown as points, $S_1^{1/2}V_1$ (○), $S_2^{1/2}V_2$ (□), and $S_3^{1/2}V_3$ (◇). Lines represent fits of the SVD temporal amplitudes, $S_1^{1/2}V_1$ (−), $S_2^{1/2}V_2$ (- - -), and $S_3^{1/2}V_3$ (•••), calculated from the MLFER kinetic model.

the hybrids and normal HbCO was found in a previous photodissociation kinetic study (*14*).) These values for the amplitudes a_{hybrid} and a_{native} led to an estimate of ∼1.0 kcal/mol for the free energy difference between the T_2 and R_2 microstates of the hybrids (from $\Delta G_c(T_2) - \Delta G_c(R_2) = -RT \cdot \ln(a_{\text{native}}/a_{\text{hybrid}} - 1)$, an expression that for simplicity neglected the greater intensity of the photolysis difference spectrum of the R state relative to the blue-shifted T state). If one neglects for the moment the perturbation of microstate energies that accompanies cobalt−iron substitution, this value provides a rough estimate of the difference between the energy of the ^{23}T and ^{24}T microstates (and thus the probably isoenergetic ^{22}T microstate as well) and the energy of the R_2 microstates in the native stripped protein. Addition of this value to the previously measured cooperative free energy of the R_2 microstates of Hb_ACO yields an estimated value of ∼7.5 kcal/mol for the free energy of the ^{22}T, ^{23}T, and ^{24}T microstates. The value of the latter energy is an important input to the MLFER kinetic model for native HbCO presented in the companion paper (*1*). In the present work, the estimated value of $\Delta G_c(T_2) - \Delta G_c(R_2)$ was added to the R_2 free energies of the hybrids to obtain initial values for $\Delta G_c(T_2)$, a free parameter in the MLFER kinetic modeling procedure that was optimized for each hybrid. The values of $\Delta G_c(T_2)$ optimized below for the hybrids were then used to calculate a consensus value for the $\{^{22}T,\ ^{23}T,\ ^{24}T\}$ microstate free energy of Hb_ACO via the cobalt-substitution energy transformation rules given above. This consensus

value was used in the MLFER kinetic model of normal hemoglobin presented in (*1*).

The kinetic parameters of the MLFER model optimized for the hybrid photolysis data, including those for the geminate rebinding processes, are presented in Table 3. (Note that it may be possible to model the $^{ij}\Delta G_c$ dependence of the geminate rebinding parameters g_n tabulated here by MLFERs in a manner similar to those used for the bimolecular rebinding parameters, but that was not attempted in this work. In this sense, the geminate parameters presently remain outside of the MLFER conceptual framework.) The geminate parameter values reported here did a satisfactory job of reproducing the time course of geminate rebinding (see the first several hundred nanoseconds of panel b in Figures 3−6), but the values of g_2 for both hybrids were unexpectedly small (<1 ns), given the value of 130 ns determined for Hb A_0 (*1*). It is not clear whether this indicates a real difference between the mechanism of geminate rebinding in the hybrids and that of the native protein or a shortcoming of the model in deconvoluting the geminate dynamics of the hybrid R conformer from the large background signal presented by the prephotolysis T-conformer
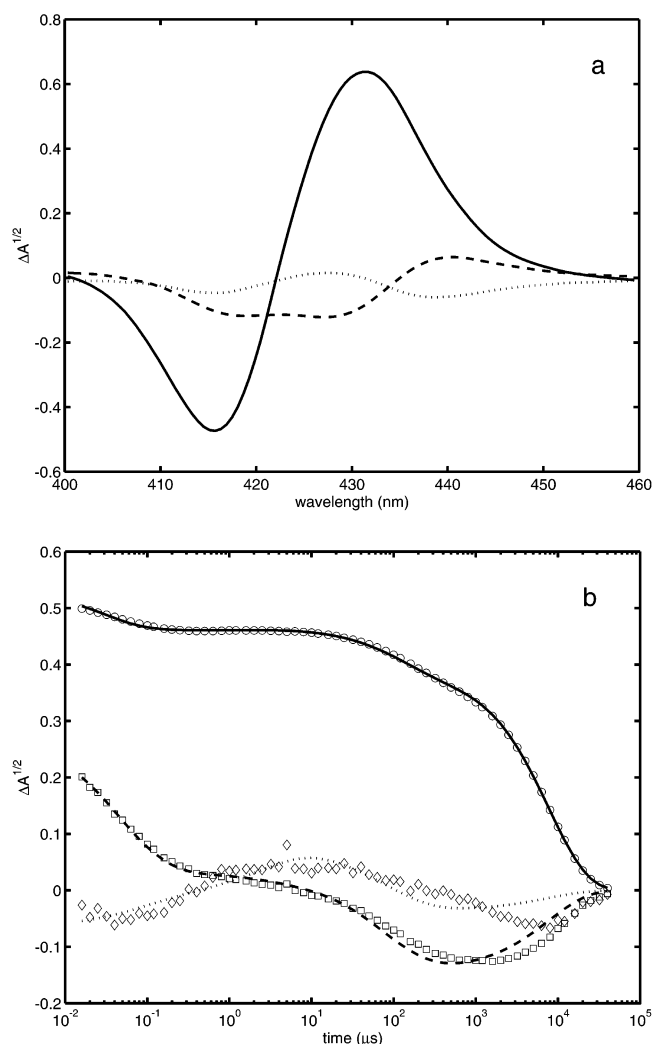
FIGURE 4: The first three SVD components of photolysis data for hybrid HbCO **23** + IHP. (a) Basis spectra, $S_n^{1/2}U_n$. (b) Temporal amplitudes, $S_n^{1/2}V_n$, and calculated fits. Components are labeled as in Figure 3 legend.

FIGURE 5: The first three SVD components of photolysis data for stripped hybrid HbCO **24**. (a) Basis spectra, $S_n^{1/2}U_n$. (b) Temporal amplitudes, $S_n^{1/2}V_n$, and calculated fits. Components are labeled as in Figure 3 legend.

population in the IHP-bound samples (which would tend to lower the effective signal-to-noise ratio compared to that in the Hb$_A$CO study).

The $^{01}k_{RT}$ value reported for hybrid **23** in Table 3 was not very different, within the reported uncertainties, than the value found for normal hemoglobin (*1*). The thermodynamic driving forces for the R$_0$ → T$_0$ transition also appear to be very similar in this hybrid and unmodified HbCO (compare the R$_0$ → T$_0$ free energy differences shown in Figure 9a and in Figure 2 of ref *1*). Thus, we find here a reasonably close correspondence in the rate constants for isoenergetic quaternary structural transitions of differently metalated hemoglobins. This finding supports the idea underlying this work that cobalt substitution preserves the essential features of hemoglobin cooperativity represented by the MLFER parameters. Similarly, the $^{01}k_{RT}$ value reported for hybrid **24** is smaller than that for **23** by a factor of 2.4. This factor matches closely the ratio that would be predicted by a MLFER linking the kinetics of the hybrids by using the R$_0$ → T$_0$ transition free energies, 6.6 vs 4.2 kcal/mol for **23** and **24**, respectively (see Table 1 and Figure 9), and the α_{RT} value of normal hemoglobin (0.2). Because the two hybrids were modeled independently, using the α_{RT} value of normal hemoglobin in a separate MLFER modeling procedure for each hybrid,

the latter correspondence provides further evidence for the apparent insensitivity of α_{RT} to the presence (and α- vs β-chain location) of iron−cobalt substitution.

The MLFER parameters for CO recombination were insensitive to α,β chain differences, the two hybrids having essentially identical values for α_{CO} (0.6) and k_R (both the pseudo first-order rate constants in Table 3 corresponding to a bimolecular rate constant for CO binding of 6 μM^{-1} s^{-1}). These parameters do seem more perturbed by the substitution of iron with cobalt than the allosteric parameters α_{RT} and $^{01}k_{RT}$, however. The α_{CO} value for the hybrids is about 30% larger than that for normal hemoglobin, which is clearly significant. The increase suggests that the transition state for CO binding becomes somewhat more product like with iron−cobalt substitution. The CO rebinding rate constants of the hybrids may also be perturbed, but given the relatively large uncertainties in determining the rate constants, it is not clear if the difference from the value for fully ferrous hemoglobin is very significant.

Allosteric effector interactions were measured in the hybrids with two parameters, $\Delta G_{IHP}(T_0)$ and $\Delta G_{IHP}(T_2)$, that allowed for a heme-ligation dependence to the free energy of IHP binding to the tetramer, as has been observed for
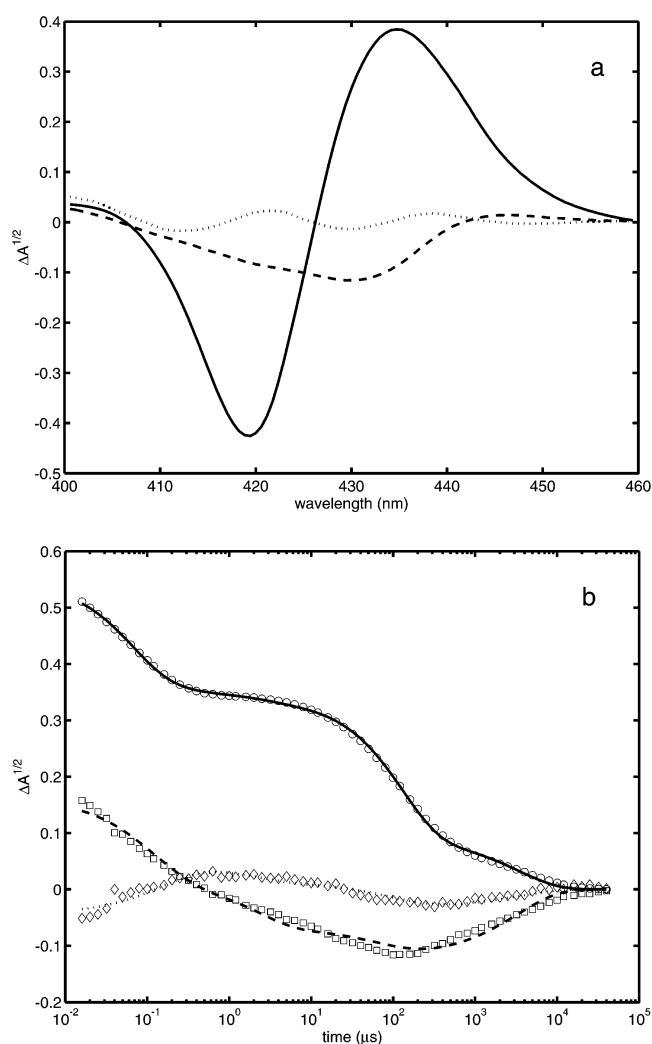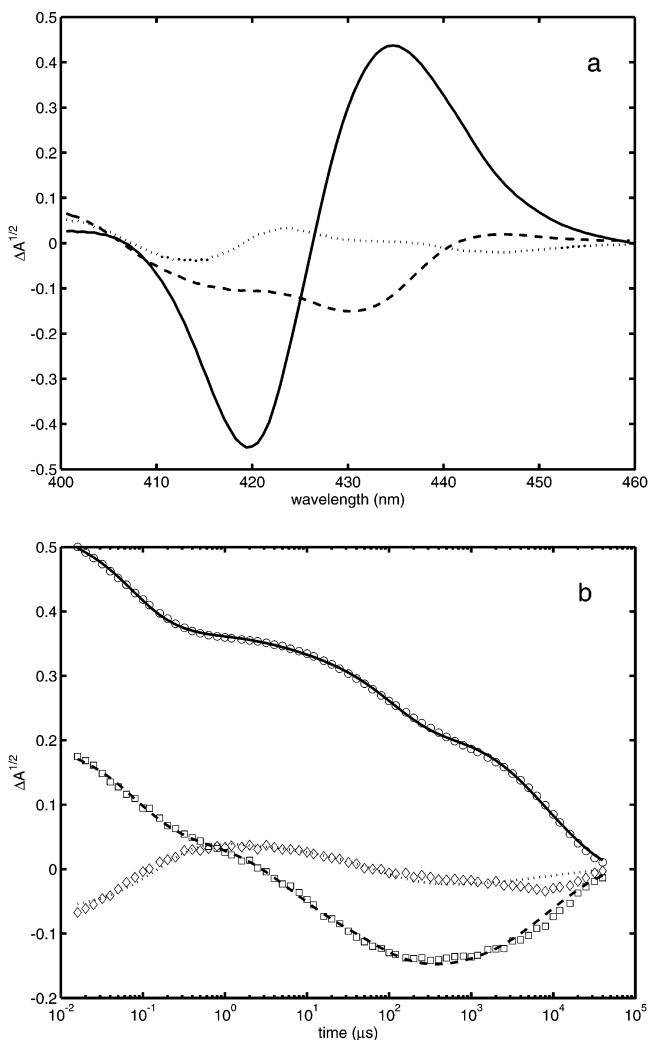
FIGURE 6: The first three SVD components of photolysis data for hybrid HbCO **24** + IHP. (a) Basis spectra, $S_n^{1/2}U_n$. (b) Temporal amplitudes, $S_n^{1/2}V_n$, and calculated fits. Components are labeled as in Figure 3 legend.

Table 2: Effect of IHP on Observed Time Constants and Spectral Amplitudes from Simple 6-Exponential-Decay Global Fitting of Cobalt−Iron Hybrid HbCO Photolysis Data[a]

hybrid[b]	τ_1	τ_2	τ_3	τ_4	τ_5	τ_6
23	0.024	0.086	3.3	47	170	7300
	(0.23)	(0.14)	(0.03)	(0.12)	(0.15)	(0.32)
23 + IHP[c]	0.055	0.45	25	160	3500	8800
	(0.11)	(0.03)	(0.02)	(0.15)	(0.08)	(0.61)
24	0.028	0.12	2.4	60	240	4900
	(0.16)	(0.22)	(0.03)	(0.19)	(0.28)	(0.12)
24 + IHP[c]	0.042	0.18	7.3	62	420	12000
	(0.16)	(0.15)	(0.07)	(0.15)	(0.11)	(0.34)

[a] Time constants are in μs, fractional amplitudes (proportional to the vector norms of the decay spectra) are listed in parentheses. [b] Conditions: 120 μM heme, pH 7.4, 0.1 M Tris, 0.1 M NaCl, 1 mM EDTA, 20 °C. [c] 2 mM IHP.

DPG and IHP binding with native protein (*7*, *11*). The binding of IHP to the α-chain substituted hybrid, **24**, was found to resemble more closely that of normal hemoglobin in both strength and ligation dependence than that of the β-chain substituted hybrid, **23**. The **24** ΔG_{IHP} values (see Table 3) were decreased from those of Hb A_0 by $\sim$30% and, as in normal hemoglobin, the binding of two CO ligands roughly halved the IHP binding energy. In contrast, the

FIGURE 7: Model-independent decay spectra calculated from a 6-exponential fit to photolysis data for hybrid **23** (a) stripped and (b) + IHP. Spectra for decay τ's: τ_1 (—), τ_2 (- - -), τ_3 (- • -), τ_4 (•••), τ_5 (— —), τ_6 (- — -) (numbering as in Table 2).

energy of IHP binding to deoxy **23** appeared to be less than half of that for Hb A_0, and no ligation dependence was observed. These results suggest that metal substitution at the β-chain heme site more strongly perturbs IHP binding to the tetramer than does substitution at the α chain. This observation is consistent with the principal role that β-chain contacts play in stabilizing IHP at the effector binding site in the central cavity of the tetramer (*15*), the structural perturbation imposed by metal substitution being expected to propagate most directly via the tertiary structure of the affected chain to the effector binding site.

The microstate rate constants shown in Table 4 afford a more complete look at the allosteric kinetics of the hybrids and the combined effects of cobalt substitution and IHP effector described above in the context of the free parameters $^{01}k_{RT}$, $\Delta G_{IHP}(T_0)$, and $\Delta G_{IHP}(T_2)$. The $^{ij}k_{RT}$ rate constants calculated for stripped **23** were on average $\sim$40% smaller than the rate constants for the corresponding microstates in Hb$_A$CO, whereas those for stripped **24** are $\sim$70% smaller. The greater perturbation of allosteric rates in the latter hybrid is consistent with the greater perturbation of microstate energies imposed by cobalt substitution at the α chains, which results in a smaller thermodynamic driving force. Examining the hybrid rate constants in the presence of IHP
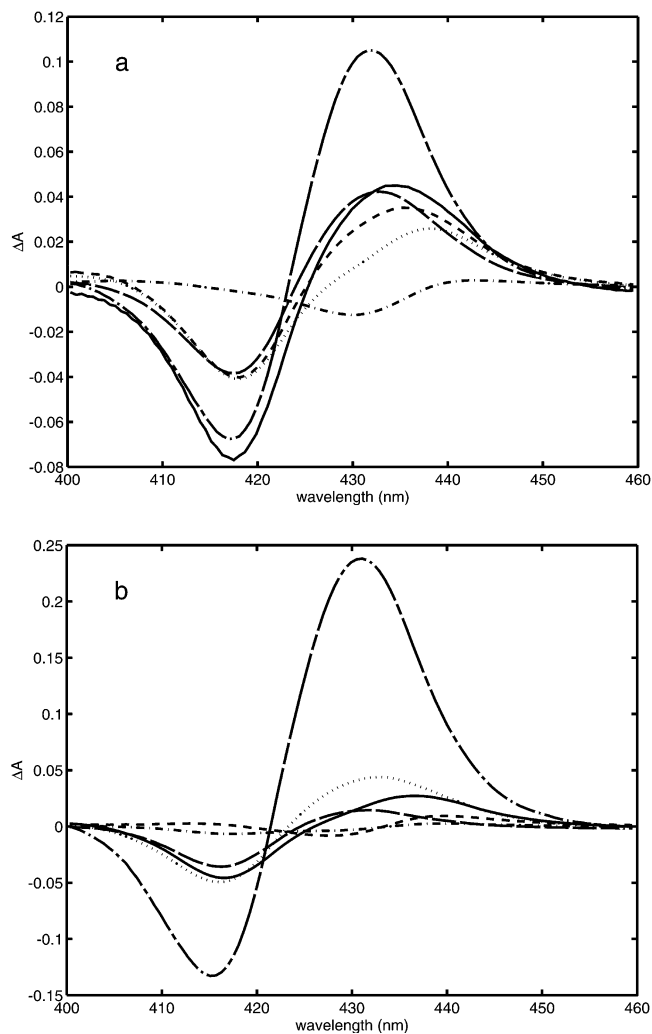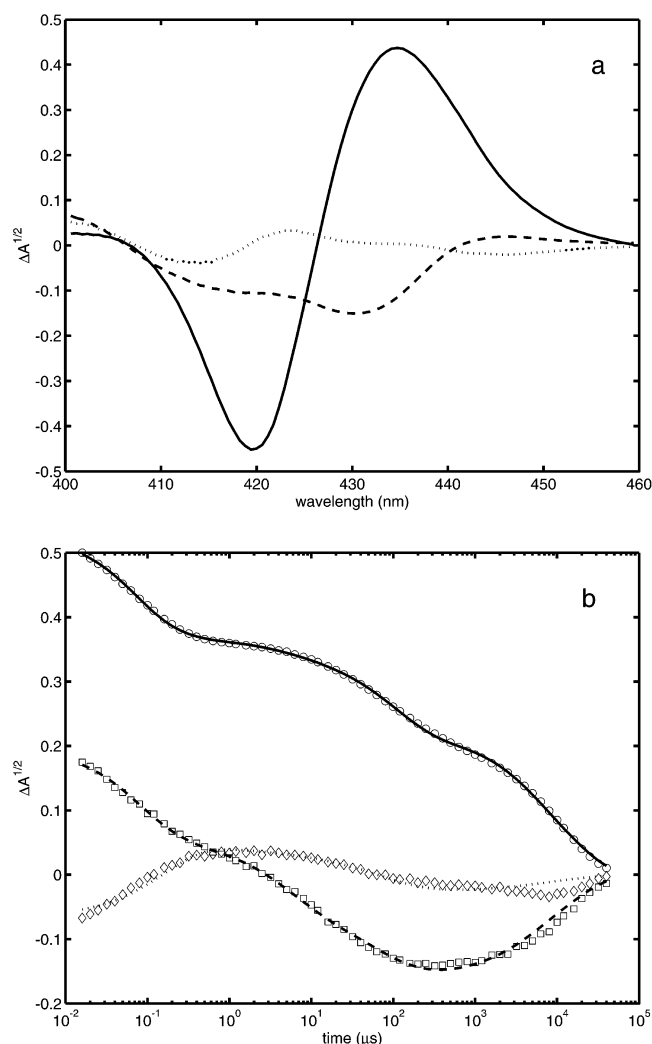
FIGURE 8: Model-independent decay spectra calculated from a 6-exponential fit to photolysis data for hybrid **24** (a) stripped and (b) + IHP. Spectra labeled as in Figure 7 legend.

shows that the latter effect is nearly offset by the greater perturbation on IHP binding imposed by metal substitution at the β chains. The net effect is that the R $\rightarrow$ T microstate rate constants for the **23** and **24** hybrids are more similar to each other in the presence of IHP. They are thus reduced by more similar amounts, 70 and 80%, respectively, from the corresponding rates in normal hemoglobin.

The bimolecular CO recombination rate constants calculated for the hybrid T microstates (Table 5) tended to cluster together very closely compared to those for native hemoglobin (the latter varied over a very large range that approached that traditionally assigned to the difference between R- and T-state recombination rate constants) (*1*). This lack of a dramatic cooperativity effect on ligand binding within the hybrid T microstates is consistent with the absence of the [21] ligation microstate in the set of states available to the symmetric Fe−Co hybrids. Without the presence of the asymmetrically liganded ^{21}T microstate and its anomalously low cooperative energy in the symmetric Fe−Co hybrids, the cooperative energies of the T microstates increase relatively evenly with ligation (see Figure 9). Such an evenly spaced "ladder" of cooperative energies leads, via thermodynamic linkage, to similar recombination rates for the T microstates within the MLFER model. Thus, the ligand-

Table 3: Initial and Optimized Values of MLFER Kinetic Model Parameters for Photolyzed Co−Fe Hybrid HbCO[a]

hybrid	parameter	trial[d]	optimized[e]
23	g_1[b]	0.02	0.03
	g_2[b]	0.12	0.0
	g_3[b]	0.05	0.08
	$^{01}k_{RT}$	2×10^4	$9.0 \pm 1.0 \times 10^3$
	α_{CO}	0.5	0.60 ± 0.01
	k_R[c]	5×10^3	$6 \pm 2 \times 10^3$
	$^{11}\Delta G_c(T)$	3.4	3.8 ± 0.1
	$^{23}\Delta G_c(T)$	7.9	7.6 ± 0.3
	$\Delta G_{IHP}(T_0)$	-5.0	-2.2 ± 0.1
	$\Delta G_{IHP}(T_2)$	-5.0	-2.0 ± 0.1
24	g_1[b]	0.02	0.06
	g_2[b]	0.12	0.0
	g_3[b]	0.05	0.08
	$^{01}k_{RT}$	2×10^4	$3.9 \pm 0.5 \times 10^3$
	α_{CO}	0.5	0.58 ± 0.01
	k_R[c]	5×10^3	$6 \pm 2 \times 10^3$
	$^{12}\Delta G_c(T)$	5.8	5.4 ± 0.1
	$^{24}\Delta G_c(T)$	8.0	8.7 ± 0.3
	$\Delta G_{IHP}(T_0)$	-5.0	-3.7 ± 0.1
	$\Delta G_{IHP}(T_2)$	-5.0	-1.6 ± 0.1

[a] Rate constants are in s^{-1}. [b] Time constants are in μs. [c] Pseudo-first-order rate constant (1 atm CO). [d] Trial values used to determine the starting point for optimization procedures. [e] Statistical average of $N = 100$ optimizations run using $^{ij}\Delta G_c$ and ΔG_{IHP} energy inputs that were randomly varied by $\pm$ 0.3 kcal (standard deviation) from values given in text.

binding behavior of the symmetric hybrids is actually much more similar to that expected from the traditional two-state model of hemoglobin allostery than is that of native hemoglobin.

The addition of IHP had little effect on the CO rebinding rate constants calculated for the **23** hybrid (see Table 5), a consequence of the apparent insensitivity of IHP binding to CO ligation in this hybrid. Lowering the energy of all the T microstates equally, the addition of IHP did not change the cooperative energy penalties for ligand binding. The interaction of IHP with the **24** hybrid, on the other hand, does appear to decrease with CO ligation, which increases the cooperative energy penalty for both ligand binding steps. Because the model assumed a linear dependence of IHP binding energy on the extent of CO ligation, the cooperative energy penalties of both CO binding steps were increased equally. This was reflected in the equal fall off of the calculated CO binding rate constants for the ^{01}T and ^{12}T microstates of **24** upon addition of IHP.

A graphical comparison of the rebinding kinetics in normal and Fe−Co hybridized HbCO (Figure 10) shows a much tighter clustering of the T-state rebinding rate constants in the hybrids relative to the native protein (all of the points indicate T-state rate constants except for the R-state rate constants corresponding to $^{ij}\Delta G_{CO} = -11.8$ kcal/mol), despite the additional dispersion associated with the addition of IHP to **24**. The bimodal distribution of R and T-state rebinding rates shown for the hybrids, reminiscent of a simple two-state model, is not evident in native HbCO (although some of the dispersion in the latter points is again due to the effect of IHP). Although the uncertainties in the rate constants are relatively large, the difference in slope between the line fitting the aggregate hybrid points and the line for Hb A$_0$ seems significant, again suggesting that cobalt substitution significantly perturbs the transition state for the
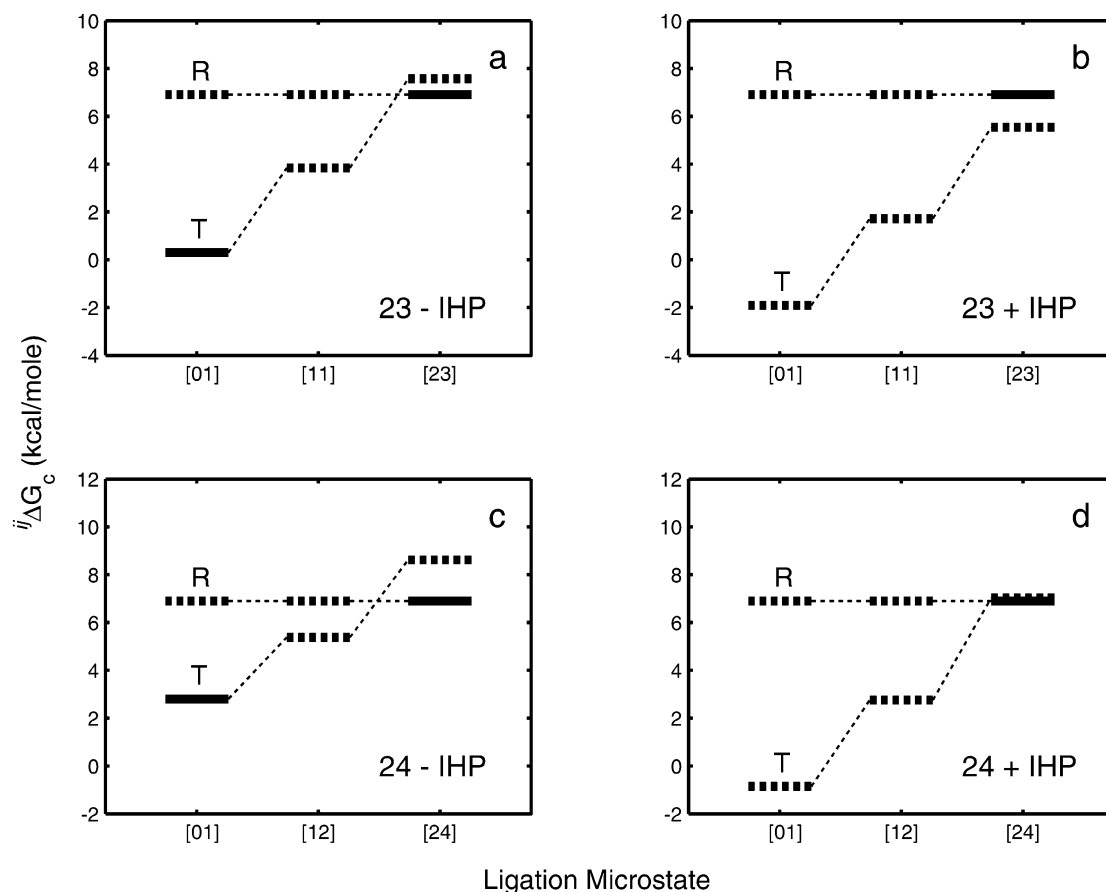
FIGURE 9: Scheme of cooperative energies, ΔG_c, for ^{ij}R and ^{ij}T microstates of Hb$_{23}$CO (a) stripped and (b) +IHP, and Hb$_{24}$CO (c) stripped and (d) +IHP. Experimental values (solid) were taken from data of Huang and Ackers (5). Remaining values (dashed) were either fixed inputs for MLFER kinetic model, estimated as discussed in text, or optimized parameters.

Table 4: Microstate R→T and T→R Quaternary Transition Rate Constants Calculated from MLFER Model[a]

| | | $^{ij}k_{RT}$ | | $^{ij}k_{TR}$ | |
hybrid	[ij]	stripped	IHP	stripped	IHP
23	[01]	$9 \pm 1 \times 10^3$	$1.9 \pm 0.2 \times 10^4$	0.10 ± 0.05	$4 \pm 3 \times 10^{-3}$
	[11]	$2.6 \pm 0.2 \times 10^3$	$5.5 \pm 0.6 \times 10^3$	14 ± 3	0.7 ± 0.1
	[23]	$7.2 \pm 0.4 \times 10^2$	$1.4 \pm 0.1 \times 10^3$	$3 \pm 1 \times 10^3$	$1.5 \pm 0.4 \times 10^2$
24	[01]	$3.9 \pm 0.5 \times 10^3$	$1.4 \pm 0.3 \times 10^4$	3 ± 2	$2 \pm 1 \times 10^{-2}$
	[12]	$1.5 \pm 0.2 \times 10^3$	$3.8 \pm 0.4 \times 10^3$	$1.0 \pm 0.6 \times 10^2$	2.5 ± 1.5
	[24]	$5.2 \pm 0.7 \times 10^2$	$9 \pm 1 \times 10^2$	$1.0 \pm 0.5 \times 10^4$	$1.0 \pm 0.4 \times 10^3$

[a] Rate constants are in s^{-1}.

Table 5: Microstate Bimolecular CO Recombination Rate Constants Calculated from MLFER Model for Iron−Cobalt Hybrids 23 and 24[a]

| | **23** | | **24** | |
	stripped	IHP	stripped	IHP
k_R	6 ± 2	6 ± 2	6 ± 2	6 ± 2
$^{01,11}k_T$	0.14 ± 0.05	0.13 ± 0.04		
$^{01,12}k_T$			0.4 ± 0.1	0.12 ± 0.04
$^{11,23}k_T$	0.12 ± 0.04	0.10 ± 0.03		
$^{12,24}k_T$			0.4 ± 0.1	0.13 ± 0.4

[a] Rate constants are in μM^{-1} s^{-1}.

CO rebinding reaction at the ferrous heme sites in Fe−Co hybrids.

The optimized values of the T$_1$ cooperative free energies, $^{11}\Delta G_c$ and $^{12}\Delta G_c$, of the respective (stripped) hybrids, **23** and **24**, each fell within the ranges established by our initial estimates (see Table 1). These estimates were based on cobalt-substitution transformation rules derived from equilibrium thermodynamic data. Hence, this concordance further validated the assumption implicit in the present work that these rules can be usefully extrapolated to the estimation of energies of nonequilibrium microstates. (Note that the present work applied the rules to T microstates, whereas the R-microstate energies were assumed to be relatively insensitive to perturbations.) These rules were thus employed again below to calculate the cooperative free energies of T$_2$ microstates of the native protein from those of the hybrids.

Initially estimated roughly above, more precise values for the cooperative free energies of the doubly liganded T states of each hybrid, $^{23}\Delta G_c$ and $^{24}\Delta G_c$ respectively, are provided by the MLFER optimized values given in Table 3. Applying the iron → cobalt transformation rules to these energy values to calculate the cooperative free energies of the corresponding microstates in Hb A$_0$ gives values of 7.9 + (0) = 7.9 (no perturbation rule applies) and 8.7 − 2(0.4) = 7.9 (rule 2)
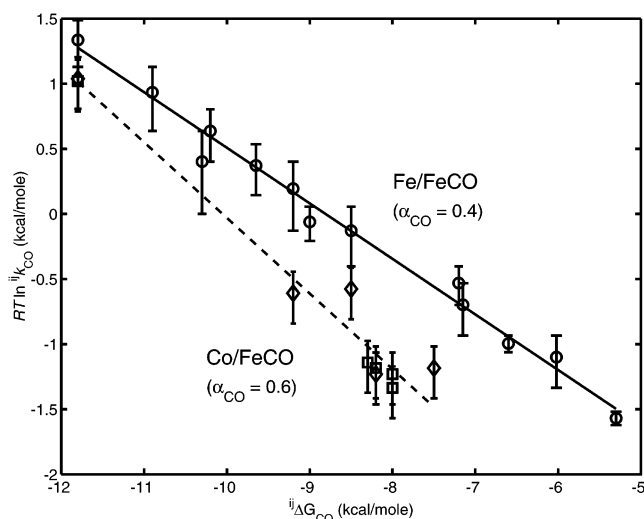
FIGURE 10: MLFER plots for ligand rebinding rates in native Fe/FeCO ($-$) and symmetric Co/FeCO hybrid (- -) hemoglobins. Plotting $RT \ln({}^{ij}k_{CO})$, where the ${}^{ij}k_{CO}$ are the rebinding rate constants for the ${}^{ij}R$ and ${}^{ij}T$ microstates of native ($\bigcirc$), or **23** hybrid ($\square$) and **24** hybrid ($\diamond$), (with and without IHP) vs the free energy of rebinding gives a straight line whose slope is equal to $-\alpha_{CO}$. Energies were calculated from the thermodynamic linkage relation ${}^{ij}\Delta G_{CO} = {}^{ij}\Delta G_c(\text{product}) - {}^{ij}\Delta G_c(\text{reactant}) + \Delta G_{CO}^{D}$, where the ligand binding free energy of free dimer, ΔG_{CO}^{D}, was -11.8 kcal/mol. Lines represent a linear least-squares fit to the points for native or hybridized HbCO with the indicated negative slopes (the R-state rebinding rate for each metalation species was weighted only once in the fits).

kcal/mole, respectively. The close agreement between the two estimates is gratifying, given that Huang and Ackers (*5*) did not observe α,β chain effects in the cooperative free energies of Hb$_A$CO; thus, ^{23}T and ^{24}T (and ^{22}T, which does not have an analogue in the symmetric hybrids) are expected to be isoenergetic in normal HbCO.

DISCUSSION

The symmetry rule model of hemoglobin allostery has been based upon the observation of a pattern in the cooperative free energies of the 10 ligation "microstates" accessible to equilibrium experiments, a pattern pervasive across a variety of ligation analogue systems (*5, 16−23*). In this pattern, the ^{21}T microstate (both ligands bound to the same $\alpha\beta$ dimer in the T-state tetramer) stands out among the observed microstates in that it is much lower in energy than other doubly liganded T microstates, ^{2n}T ($n \neq 1$), indicating that the manner in which ligands are distributed between dimers crucially affects the cooperative energy of the tetramer. The lower energy of ^{21}T is attributed in the symmetry rule model to the lower energy penalty exacted by perturbing the structure of one dimer in the T quaternary state, as opposed to perturbing both dimers. However, just how much lower has remained an open question, because the other T₂ microstates are not observed at equilibrium. They are apparently higher in energy than their R₂ counterparts that are observed (at least in hemoglobin stripped of effectors), as are the T₃ and T₄ microstates. The major break in stability that tips the allosteric equilibrium from the T to R form thus occurs when ligand binding perturbs both dimers, that is, dimer perturbation by ligand binding becomes symmetrical across the tetramer. As we are unable to observe

the ^{2n}T ($n \neq 1$) microstates directly, equilibrium measurements of cooperative energies have provided only a lower limit to the putative T₂ microstate energy gap (${}^{2n}\Delta G_c(T) - {}^{21}\Delta G_c(T) > {}^{2n}\Delta G_c(R) - {}^{21}\Delta G_c(T) = 2.3$ kcal/mol (*5*)).

The pivotal role of the T₂ energy gap in the symmetry rule led us to undertake kinetic studies of the iron−cobalt HbCO hybrids as a means to measure the cooperative energies of the "missing" ^{2n}T microstates. If these energies are not too high, then the CO complex of the **23** or **24** hybrid will comprise a mixture of the ^{23}T and ^{23}R or ^{24}T and ^{24}R microstates, respectively, at equilibrium. The very different kinetic properties of R and T states after ligand photodissociation then provide a sensitive assay of the $L_2 = [T_2]/[R_2]$ equilibrium constant and thus the free energy of the ^{23}T or ^{24}T microstate. Using the different geminate recombination kinetics of the R and T states, a rough estimate of the range of free energy values $-RT \cdot \ln L_2 \approx -1$ to 1 kcal/mol was obtained above for the hybrid samples with and without IHP, values consistent with the assumption that each sample contained a finite equilibrium of R and T conformers. This finding is also consistent with the results of a previous CO photodissociation study of these hybrids, which found similar populations of R and T conformers in the equilibrium complex of **23** (*14*).

With this simple and relatively transparent validation of the kinetic assay approach in place, we applied the novel MLFER kinetic model to obtain more precise values of the ^{23}T and ^{24}T free energies. In doing so, however, we found that initial attempts to model the hybrid photolysis data with a procedure that optimized the value of the allosteric MLFER coefficient α_{RT} as a free parameter did not converge well. This was in contrast to the successful optimization of the same parameter in a MLFER model fit of similar data for normal HbCO presented in the companion article (*1*). The poor convergence of the unconstrained α_{RT} parameter in the hybrid MLFER model was probably due to several factors. A principal factor was the low population of R conformers present in the prephotolysis hybrid samples, particularly those containing IHP, compared with normal HbCO. Thus, the effect of the α_{RT} parameter in modulating the R→T transition rate was diluted in the overall photolysis kinetics of the hybrid samples, which tended to be dominated by bimolecular recombination of CO with the T state. A second factor was the introduction of additional free parameters, $\Delta G_{IHP}(T_0)$ and $\Delta G_{IHP}(T_2)$, to the MLFER models of the hybrids, accounting for the extent of IHP binding and its effect on microstate energies. A third factor was the smaller effect of IHP on the hybrids, which provided both less complete IHP binding and less of a shift in the R→T driving force in those tetramers that did bind IHP with which to assess the MLFER α_{RT} value. Finally, a fourth factor was the somewhat weaker dimer−dimer association reactions of the hybrids, which resulted in a higher fraction of (nonallosteric) R-like dimers in the hybrid samples (15 vs 10%). All these factors would tend to contribute to making the value of α_{RT} effectively underdetermined by the data. Nonetheless, we were able to obtain good convergence in the hybrid modeling procedures by fixing the value of α_{RT} at the value for normal HbCO, 0.2. This extrapolation of the Hb A_0 value to the hybrids was supported by the observation of a self-consistency relation in the ${}^{01}k_{RT}$ values obtained for **23** and **24**. The latter were found to be related by an unconstrained MLFER α

value that was very close to the HbACO value. (This relationship was also robust with respect to variations in the constrained α_{RT} value: MLFER analyses using α_{RT} values of 0.15 or 0.25 to fit each hybrid's kinetics independently still found that their $^{01}k_{RT}$ rate constants were related by an α value close to 0.20, results not shown.)

The apparent congruence of α_{RT} values for the iron−cobalt hybrids and normal hemoglobin suggests that cobalt substitution does not significantly perturb the nature of the allosteric transition state. This means that even though cobalt substitution significantly perturbs the cooperative energies, the effect of those energy changes on R→T rates is still mediated by their effect on the activation free energy required to reach the same R-like transition state. On the other hand, the larger value of α_{CO} found for the hybrids (0.6) compared with normal hemoglobin (0.4) implies that cobalt substitution alters the CO recombination reaction pathway so as to make the transition state more like the product state.

Previous structural and chemical studies have investigated the manner in which cobalt substitution preserves core elements of the allosteric mechanism while perturbing the cooperative energies, particularly those of the α-substituted hybrids. Replacing all four irons with cobalt produces a tetramer that binds oxygen with only slightly less cooperativity than ferrous Hb (*24*). This preservation of cooperativity occurs despite the smaller displacement of the metal from the heme plane in cobaltous deoxyHb (*25*). The relatively small effect of the cobalt-heme displacement perturbation on cooperativity has been attributed to a compensating increase in the length of the cobalt-imidazole nitrogen bond connecting the heme site via the proximal histidine to the F helix and the dimer-dimer interface, these structural elements and their interactions constituting the core of the allosteric mechanism. However, the perturbation imposed by α-metal substitution is clearly greater than that of β substitution, as evident in the cooperative free energies of **23** and **24** (see Figure 9) and the other cobalt−iron hybrids (*5*). The perturbation strength, as measured by a concomitant increase in β subunit ligand affinity, of α(Fe → M) substitution with M = Co, Ni, and protoporphyrin (no metal) was correlated with the intrinsic strength of the metal-histidine bond by Fujii et al. (*26*). The cobalt-imidazole bond is stronger than that of iron, and an increase in affinity for the first ligand accompanies Fe → Co substitution. In contrast, metal substitution at the β subunits has little effect on the ligand affinity of the α subunits. Thus, the different sensitivities of the chains to metal substitution suggests that α chains are less able than β chains to accommodate the smaller displacement from the heme plane of the cobalt atom (compared with iron) in the T quaternary state, perhaps due to a greater constraint on the metal-histidine bond geometry imposed by the α-chain conformation. Such a constraint would explain the apparent correlation of conformational strain energies in α-substituted hybrids (destabilizing $^{ij}\Delta G_c(T)$ values so as to increase ligand affinity) with metal-histidine bond strength that is implied by the results of Fujii et al.

The lack of α,β chain differences observed previously in the $^{ij}\Delta G_c$ values of fully ferrous HbA has suggested that the affinities and kinetics of ligand binding are probably very similar for the two chain types. Nevertheless, it did not rule out the possibility of a difference in the intrinsic ligand binding kinetics of the chains. That possibility, however, does

appear to be discounted by the identical k_R values found here for the two hybrids. The observation of identical intrinsic CO binding rate constants for the $(\alpha_{Co}\beta_{FeCO})_2$ and $(\alpha_{FeCO}\beta_{Co})_2$ hybrids strongly suggests equivalent CO rebinding kinetics for the α and β chains in fully ferrous tetramer. This is also consistent with previous observations of the geminate and bimolecular recombination reactions in these hybrids, which found little difference between α and β chain kinetics (*14*).

The $^{ij}\Delta G_c$ values for the T_2 microstates determined here have several ramifications. First, the equality of the energies of ^{23}T and ^{24}T calculated for normal HbCO extends from equilibrium to metastable microstates the observation of a relative insensitivity of cooperative free energies to α,β chain differences. This observation implies that the remaining "missing" T_2 microstate, ^{22}T, should also be very close in energy to ^{23}T and ^{24}T. Second, this value of $^{2n}\Delta G_c(T)$ (7.9 kcal/mol) provides an input that is pivotal in accurately determining a MLFER model for normal HbCO (*1*). With this value, that MLFER model was able to elucidate several surprising features of normal HbCO kinetics that have not been reported by previous workers, including cooperativity of ligand binding within the T microstates, the concomitant emergence of the ^{21}T microstate as a kinetic bottleneck in CO recombination reactions, and a suggested reassignment of different R-state CO recombination rate constants traditionally attributed to α,β chain differences to R-state and T_1 + CO → ^{21}T recombination reactions instead. Moreover, it was able to do so with a minimum of free parameters and with a better quality of fit than simple two-state models that neglect the T_2 energy gap.

The ^{2n}T cooperative energies determined from the hybrid photolysis kinetics give us the most important piece missing heretofore from the microstate energy picture of HbCO. To the 10 equilibrium microstate energies obtained from thermodynamic measurements, we can now add the three metastable ^{2n}T microstates determined here and the seven metastable states ^{01}R, ^{11}R, ^{12}R, ^{21}R, ^{31}T, ^{32}T, and ^{41}T estimated in ref *1* to paint a complete picture of all 20 possible combinations of ligation and quaternary conformation (see Figure 2 in ref *1*). This represents the first quantitative determination of all the stable and metastable minima on a free energy landscape for the allosteric and bimolecular ligand recombination reactions of hemoglobin. Furthermore, by using the MLFER paradigm, we can now calculate the heights of all the saddle points on the landscape connecting those minima from the minima free energies and a small number of experimentally determined kinetic parameters.

In particular, we now have a picture of the entire "ladder" of T microstates reflecting the detailed effects of ligand number and placement on the cooperative free energies (albeit the two highest rungs, corresponding to T_3 and T_4, are the least well determined). We find that the value of the T_2 energy gap is $^{2n}\Delta G_c(T)$ − $^{21}\Delta G_c(T)$ = 3.7 kcal/mol. Similarly, when binding a second ligand to the tetramer, the cooperative free energy penalty for binding at the unliganded dimer is $^{2n}\Delta G_c(T)$ − $^{11}\Delta G_c(T)$ = 4.6 kcal/mol or $^{31}\Delta G_c(T)$ − $^{21}\Delta G_c(T) \approx 5.2$ kcal/mol. These estimates of the energetic cost of perturbing an unliganded dimer are roughly similar to the previous estimate available from equilibrium measurements, $^{11}\Delta G_c(T)$ − $^{01}\Delta G_c(T)$ = 3.3 kcal/mol, and are significantly greater than the cost of adding a second ligand to the same dimer, $^{21}\Delta G_c(T)$ − $^{11}\Delta G_c(T)$ = 0.9 kcal/mol, or

$^{31}\Delta G_c(T) - ^{2n}\Delta G_c(T) \approx ^{41}\Delta G_c(T) - ^{31}\Delta G_c(T) \approx 1.5$ kcal/mol. Thus, the cooperative energies determined from our kinetic results extend the pattern of dimer conformational energies observed in previous thermodynamic experiments to the metastable microstates as well. In other words, we can now state for the entire ladder of T microstates that the major increments in cooperative energy occur upon binding of the first ligand to an unliganded dimer, the perturbation of dimer structure accompanying the binding of a second ligand apparently being much smaller, irrespective of the ligation status of the other dimer. This is in contrast to the equally spaced ladder of T microstate energies proportional to ligation number ($^{ij}\Delta G_c = l \cdot \Delta\Delta G_c^{\text{two-state}}$, where $\Delta\Delta G_c^{\text{two-state}} \approx 11/4$ kcal/mol and l = number of ligands) implicit in the traditional two-state model.

The cooperativity of ligand binding within the T quaternary conformation implied by previous equilibrium measurements of $^{ij}\Delta G_c$ values for HbCO and HbO$_2$ is explicitly extended to the metastable T microstates of HbCO by the $^{23}\Delta G_c$ and $^{23}\Delta G_c$ values measured here. This cooperativity is further supported by the kinetic evidence for a wide dispersion in the T-microstate CO rebinding rate constants (irrespective of allosteric effector binding) found in (*1*). In other words, the kinetics of ligand rebinding to the T quaternary state appear to depend on the number and the dimer−dimer distribution of bound ligands in a manner consistent with the $^{ij}\Delta G_c$ values of Huang and Ackers (*5*). However, this feature of the symmetry rule model (and its kinetic analogue, the MLFER model) is incompatible with traditional formulations of the two-state model, which hold that all cooperativity in ligand binding is mediated by the equilibrium between two quaternary state, R and T (*27, 28*). In terms of cooperative free energies, the symmetry model incorporates the observed inequalities in energy penalties accompanying binding to different T microstates, whereas the two-state model assumes that these are all equal. Conceptually, the symmetry model implies a significant cooperativity in ligand binding that is localized to each dimer in the T conformation, reminiscent of the sequential KNF model of cooperativity (*29*), in addition to the global cooperativity mediated by the R↔T transformation. It can thus be considered a hierarchical model in which sequential cooperativity within the T-state dimers modulates the two-state equilibrium mediating global cooperativity. The earliest formulations of the two-state model by Monod et al. insisted that not only were ligand binding affinities independent of ligation within the R or T state but also that subunit structures remained symmetric within a quaternary state (*9*). In other words, subunit tertiary structure was coupled to ligation only via the global quaternary structure. The advent of more detailed mechanistic models for allostery (*30−34*) required the recognition that subunit tertiary structure is directly altered by ligand binding (*27, 35*). Similarly, the assumption that there is no intersubunit coupling between such structural changes except via the R↔T quaternary transformation appears increasingly divergent from recent thermodynamic and kinetic evidence, at least for subunits within a given dimer.

The most significant previous experimental evidence regarding the question of T-state cooperativity in hemoglobin has come from ligand binding studies of deoxy hemoglobin in crystals (*36, 37*) and sol−gels (*38*). Constrained by crystal or gel environmental forces from converting to the R state

(T→R conversion is thought to produce the cracking often observed upon oxygenation of deoxy Hb crystals), the binding of oxygen molecules to the T state is observed to conform to a linear Hill plot of saturation vs O$_2$ pressure with a slope of unity. A Hill coefficient (n_H) of unity is traditionally considered a hallmark of noncooperative binding. In comparison, solution phase Hb tetramers typically bind ligands with an $n_H \sim 3$. However, the cooperativity implied by extrapolating the $^{ij}\Delta G_c$ values observed for unconstrained HbO$_2$ and HbCO tetramers in solution to a tetramer constrained to the T-state by environmental forces is expected to incorporate both cooperative and anticooperative ligand binding steps, unlike the large preponderance of positive cooperativity associated with binding to a tetramer free to convert from T to R. The former situation may be difficult to detect with the relatively crude measure of net cooperativity represented by n_H (*23*). Essentially, the Hill coefficient represents the projection of an observed ligand binding isotherm upon a particular model of cooperativity in which all four ligands are assumed to bind simultaneously, a value of 4 representing perfect overlap with the model. It thus appears ill-defined as a gauge of intersubunit interactions that may be orthogonal to that particular model. In particular, it is not clear that ligand binding in alternating cooperative and anticooperative steps can be meaningfully compared in this manner with the simultaneous binding of all ligands. This situation is illustrated by the Hill plot for oxygen binding to a T-constrained tetramer calculated from the previously measured $^{ij}\Delta G_c$ values of the equilibrium microstates of HbO$_2$ (0, 2.9, 2.9, and 5.1 kcal/mol for the [01], [11], [12], and [21] T microstates, respectively, from Ackers et al. (*23*)), the metastable microstate energies from the MLFER model reported in the present work and in ref *1*, and the known oxygen affinity of a free hemoglobin dimer ($\Delta G_{O2}^D = -8.35$ kcal/mol O$_2$). (Although the metastable microstate energies apply to HbCO, the differences in $^{ij}\Delta G_c$ values for CO and O$_2$ are probably no larger than the effects of crystal packing forces that are necessarily neglected in comparing solution and crystal phase ligand binding.) The Hill plot calculated from the $^{ij}\Delta G_c$ values is reasonably linear, with a slope very close to unity (Figure 11a). Yet the variations in ligand binding affinities between the T-microstates giving rise to this calculated isotherm are nearly as large as those traditionally assigned to the difference between R- and T-state properties. Clearly, the Hill coefficient is insensitive to this mixture of strongly cooperative and anticooperative ligand binding steps.

Rivetti et al. concluded that there was a small positive net cooperativity in the crystalline T state, but that its effect (an ∼10% increase in n_H) was roughly canceled from the Hill plot by the effect of a 5-fold higher ligand affinity for the α-chains versus that for the β-chains, the latter effect apparently being induced by crystal forces (*37*). The latter effect can be modeled by adding a 1-kcal/mol energy penalty to the $^{ij}\Delta G_c$ values for binding O$_2$ to a β chain. The recalculated Hill plot (Figure 11b) indeed shows a canceling of the ∼10% increase in n_H calculated in the absence of this crystal effect (cf. Figure 11a). Also note that the remarkably low affinity of the crystal is also predicted by the $^{ij}\Delta G_c$ values (with the β-chain affinity correction derived from the crystal data) (see Figure 11b). Seen in this light, the crystal data is in very good agreement with the $^{ij}\Delta G_c$ values determined
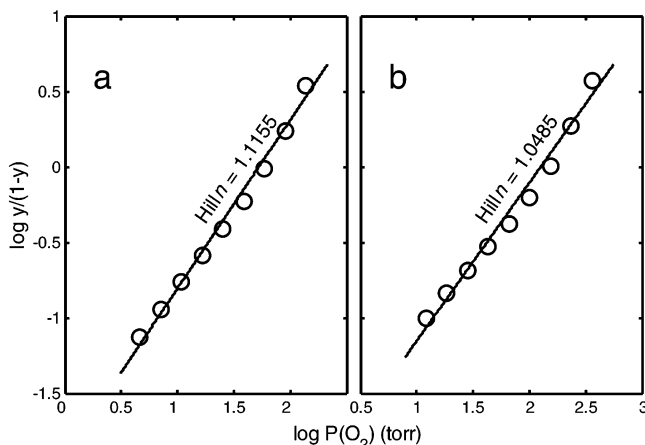
FIGURE 11: Hill plots for O_2 binding to Hb tetramer constrained in the T state calculated from $^{ij}\Delta G_c$ values given in text and the (noncooperative) ligand binding affinity of free dimers: (a) without crystal effects and (b) with a 5-fold lowering of β-chain affinity in the crystal. Values of $\ln(y/(1 - y))$, where y is the ligand binding saturation, calculated from $^{ij}\Delta G_c$ values are shown as points (o). The lines are linear least-squares fits to the points with slopes indicated (Hill coefficients).

from thermodynamic and kinetic measurements on solution phase hemoglobin, although it is not expected that the symmetry rule $^{ij}\Delta G_c$ values represent a unique fit in this regard. On balance, then, the crystal and sol−gel ligand-binding isotherm data do not appear to offer strong evidence for or against the T-state cooperativity implicit in the symmetry rule model and the microstate cooperative free energies measured in solution.

The evaluation of cooperativity models from the evidence presented by ligand binding isotherms is made difficult by the ephemeral nature of the ligation intermediates that such models attempt to describe, a circumstance that has motivated alternative approaches to the study of hemoglobin function such as measurements of dimer−dimer association reactions of ligation analogues (16) and ligand photodissociation kinetics (39). The relative insensitivity of calculated ligand-binding isotherms to significant differences between models of cooperativity can be further illustrated by comparing isotherms of equal $p50$ values calculated from (1) the $^{ij}\Delta G_c$ values for HbO_2 above; (2) a two-state model with $\Delta\Delta G_c^{\text{two−state}} = (^{41}\Delta G_c(T) - {}^{01}\Delta G_c(T))/4$, that is, equal free energy penalties summing to the same total penalty as that in (1); (3) a KNF-type sequential model in which the free energy penalty decreases linearly with each ligand bound, becoming zero for the last binding step; and (4) the naïve concerted-binding ($n_H = 4$) model (Figure 12). The binding isotherms predicted by the first three models differ by at most ±2% saturation and have very similar Hill coefficients (slope = 3.2, not shown). Note that even the most naïve model (4) is able to reproduce the behavior predicted by more sophisticated models to within ±5% saturation. The calculated concentration of tetramers in the ^{21}T microstate, in contrast, shows a marked dependence on the different energetics implied by the models (see Figure 12 inset). It is about twice as large in the symmetry rule compared with the two-state model at all oxygen pressures and is intermediate in value between these cases for the sequential model chosen (the particular choice of a sequential model is somewhat arbitrary in that one can imagine many other
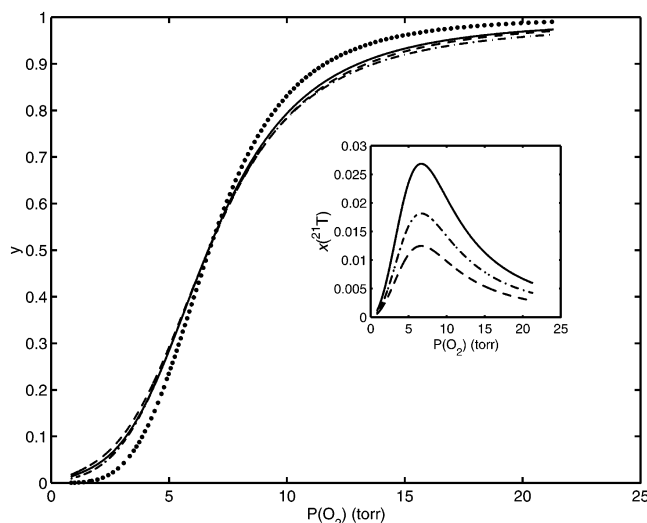

FIGURE 12: Fractional O_2 saturation (y) of hemoglobin in solution vs oxygen pressure calculated from the symmetry rule model ($^{ij}\Delta G_c$ values given in text) (−), two-state model (- -), sequential model (-·-), and concerted-binding model (...). Inset shows the corresponding calculated mole fraction of the ^{21}T microstate ([21] ligation state for the sequential model) vs oxygen pressure. (The concerted model implies no finite concentrations of intermediates.) The symmetry rule model calculation used the ligand affinity of free dimer (−8.35 kcal/mol O_2) for the value of the R-microstate affinity. The other model affinities were scaled for comparison to match the $p50$ of the symmetry rule model calculation.

sequential variations of cooperative energy penalty with ligation linking the known stabilities of the end states).

Overall, there are two separate but closely tied questions considered in this work: (1) What are the $^{ij}\Delta G_c$ values for HbCO and (2) what do those values imply for models of cooperativity? We have extracted additional $^{ij}\Delta G_c$ values for normal HbCO from the hybrid photolysis data so as to assemble, along with the values measured or inferred from previous thermodynamic studies, a reasonably complete description of its cooperative behavior. Our companion article finds that these energies provide a better description of HbCO kinetics than is available from more naïve models. With the first question largely answered by the thermodynamic and kinetic evidence, then, what are the implications for cooperativity models? The symmetry rule model has emerged as a structural interpretation of the $^{ij}\Delta G_c$ data in terms of the relative independence of each $\alpha\beta$ dimer as it is perturbed by ligand binding to the T conformer. This interpretation represents a partial relaxation of the narrower view implicit in conventional two-state models, a view that could be termed "monomer autonomy". The latter is the assumption that the perturbation of structure concomitant with ligand binding to a given subunit in a T-state tetramer remains entirely localized to that subunit. Monomer autonomy implies equal cooperative free energy penalties in the absence of significant α,β chain difference (there seems to be no evidence in solution for the difference observed in this regard in the crystal data). The symmetry rule model, on the other hand, explicitly recognizes the possibility that structural perturbation of one monomer in a dimer may be communicated to its very tightly coupled partner monomer, whereas the monomer autonomy of the traditional two-state model is assumed to largely hold for subunits on different dimers (dimers being much less tightly bound to each other than are the monomers within a dimer).

The symmetry rule model rationalizes the pattern of $^{ij}\Delta G_c$ values observed at equilibrium, in particular the surprisingly low energy of the HbCO ^{21}T microstate, 4.2 ± 0.3 kcal/mol. In a two-state model of HbCO cooperativity, this energy is expected to be $\sim$5.5 kcal/mol, half of the total cooperative free energy penalty. It also rationalizes the surprisingly high energy of the ^{11}T and ^{12}T microstates, $\sim$3.4 kcal/mol, compared to the two-state expectation, $\sim$2.8 kcal/mol. Intersubunit structural coupling within a dimer is expected to give a bigger initial penalty for binding the first ligand to a dimer and a smaller penalty for binding a second ligand to an already perturbed dimer.

In addition to rationalizing the equilibrium $^{ij}\Delta G_c$ data, the symmetry rule model also makes a testable prediction: the cooperative free energy penalty for binding two ligands will be higher than the two-state expectation given above if both dimers are perturbed. That prediction is verified by the $^{2(n\neq1)}\Delta G_c$(T) value reported here, 7.9 ± 0.3 kcal/mol. Note that the perturbations of $^{ij}\Delta G_c$ values reported here and previously, $1-2$ kcal/mol, relative to the expected two-state values are not much smaller than the increment of cooperative free energy traditionally thought to accompany the binding of a ligand to the hemoglobin tetramer.

The excellent fits to the hybrid photolysis data produced by the MLFER model are not remarkable in themselves, given that the hybrid $^{ij}\Delta G_c$(T) values have a simple two-state like ligation dependence (consistent with the absence of [21] ligation); thus, the data can be fit by a conventional two-state kinetic model (with $\Delta\Delta G_c^{\text{two-state}}$ as a free parameter) with similar accuracy (results not shown). (This contrasts with the situation for normal HbCO, in which the presence of both [21] and [2($n \neq 1$)] ligation requires a MLFER model for the best fit (*1*).) What is remarkable is the simplicity that emerges from the complexity of hemoglobin's photodissociation kinetics with the application of accurate thermodynamic information to the analysis. Hemoglobin's complexity arises from its subunit interactions, the energetics of which are described by a given set of $^{ij}\Delta G_c$ values. Applying those values via MLFERs permits a kinetic analysis that calculates all microscopic rates from a single intrinsic R $\rightarrow$ T reaction rate constant ($^{01}k_{RT} \approx 1 \times 10^4$ s^{-1}), a single intrinsic rate constant ($k_R \approx 10\ \mu$M^{-1} s^{-1}) underlying bimolecular CO rebinding to all the subunits in either quaternary conformation, and a single α_{RT} value (0.2), all of which change little, if any, with Fe $\rightarrow$ Co substitution at both α or both β hemes. The fourth MLFER parameter, α_{CO}, increases from 0.4 to 0.6, the CO rebinding transition state apparently being more sensitive to Co $\rightarrow$ Fe perturbation of adjacent subunit tertiary structure than is the R $\rightarrow$ T transition. Moreover, the MLFER parameters are independent of allosteric effector binding, allowing effectors to be incorporated naturally into the model via their effect on the $^{ij}\Delta G_c$.

The apparent robustness of this simple picture suggests that it may also be applied to systematize the study of allosteric kinetics in other hemoglobins that differ by chemical modification or protein amino acid sequence, given the necessary thermodynamic information. It also suggests a practical benefit in that the kinetics under a wide variety of effector conditions may be predicted in detail from a few experimentally determined parameters. In that regard, the present results point to the importance of further thermodynamic measurements on normal and hybrid hemoglobins to better characterize the effects of allosteric effectors on microstate energies. In particular, it seems reasonable to expect that using fixed values for the free energies of IHP binding determined from experiment (i.e., $^{ij}\Delta G_c$ values measured with IHP), rather than optimizing these values as free parameters, as was done in the present work, could better constrain the fitting and permit a completely independent optimization of the α_{RT} parameter for the hybrids.

In summary, the ligand photodissociation kinetics of symmetric Fe$-$Co HbCO hybrids were used to determine the cooperative free energy of the T quaternary conformer when one ligand is bound to each dimer, a quantity that is not available from equilibrium measurements. This energy value, along with its impact on the analysis of normal HbCO kinetics presented in our companion article (*1*), adds further support to previous thermodynamic evidence for the central finding of the symmetry rule model of hemoglobin cooperativity. That is the higher (by 4 kcal/mol) free energy of a T$_2$ microstate in which both dimers are perturbed by ligand binding compared with placing both ligands on the same dimer. This finding cannot be explained by currently accepted formulations of the two-state model. Ligand binding isotherms calculated with this T$_2$ energy gap may be considered only weakly perturbed compared with those calculated from current two-state models, as indeed are the current two-state isotherms compared with those calculated from a KNF-type model or the two-state model as originally formulated without the benefit of modern structural insights. Despite the relative insensitivity of calculated binding isotherms to the details of different models of cooperativity, the admission of increasing complexity to such models$-$when warranted by additional structural, thermodynamic, or kinetic information$-$is motivated by the opportunity for a deeper understanding of the molecular mechanisms of cooperativity and allostery.

REFERENCES

1. Goldbeck, R. A., Esquerra, R. M., Holt, J. M., Ackers, G. K., and Kliger, D. S. (2004) The molecular code for hemoglobin allostery revealed by linking the thermodynamics and kinetics of quaternary structural change. 1. Microstate linear free energy relations, *Biochemistry 43*, 12048$-$12064.
2. Szabo, A. (1978) Kinetics of hemoglobin and transition state theory, *Proc. Natl. Acad. Sci. U. S. A. 75*, 2108$-$2111.
3. Eaton, W. A., Henry, E. R., and Hofrichter, J. (1991) Application of linear free energy relations to protein conformational changes: the quaternary structural change of hemoglobin, *Proc. Natl. Acad. Sci. U. S. A. 88*, 4472$-$4475.
4. Ackers, G. K., Doyle, M. L., Myers, D., and Daugherty, M. A. (1992) Molecular code for cooperativity in hemoglobin, *Science 255*, 54$-$63.
5. Huang, Y., and Ackers, G. K. (1996) Transformation of cooperative free energies between ligation systems of hemoglobin: resolution of the carbon monoxide binding intermediates, *Biochemistry 35*, 704$-$718.
6. Ikeda-Saito, M., Yamamoto, H., and Yonetani, T. (1977) Studies on cobalt myoglobins and hemoglobins. Electron paramagnetic resonance investigation of iron$-$cobalt hybrid hemoglobins and its implication for the heme-heme interaction and for the alkaline Bohr effect, *J. Biol. Chem. 252*, 8639$-$8644.
7. Imaizumi, K., Imai, K., and Tyuma, I. (1979) The linkage between the four-step binding of oxygen and the binding of heterotropic anionic ligands in hemoglobin, *J. Biochem. (Tokyo) 86*, 1829$-$1840.
8. Marden, M. C., Hazard, E. S., Kimble, C., and Gibson, Q. H. (1987) Geminate ligand recombination as a probe of the R, T equilibrium in hemoglobin, *Eur. J. Biochem. 169*, 611$-$615.

9. Monod, J., Wyman, J., and Changeux, J. P. (1965) On the nature of allosteric transitions: a plausible model, *J. Mol. Biol. 12*, 88−118.

10. Ikeda-Saito, M. and Yonetani, T. (1980) Studies on cobalt myoglobins and hemoglobins. XI. The interaction of carbon monoxide and oxygen with α and β subunits in iron−cobalt hybrid hemoglobins, *J. Mol. Biol. 138*, 845−858.

11. Robert, C. H., Fall, L., and Gill, S. J. (1988) Linkage of organic phosphates to oxygen binding in human hemoglobin at high concentrations, *Biochemistry 27*, 6835−6843.

12. Gray, R. D. (1980) The effect of H⁺, inositol hexaphosphate, and Zn(II) on the tetramer−dimer equilibrium of liganded hemoglobin, *J. Biol. Chem. 255*, 1812−1818.

13. Murray, L. P., Hofrichter, J., Henry, E. R., Ikeda-Saito, M., Kitagishi, K., Yonetani, T., and Eaton, W. A. (1988) The effect of quaternary structure on the kinetics of conformational change and nanosecond geminate rebinding of carbon monoxide to hemoglobin, *Proc. Natl. Acad. Sci. U. S. A. 85*, 2151−2155.

14. Hofrichter, J., Henry, E. R., Sommer, J. H., Deutsch, R., Ikeda-Saito, M., Yonetani, T., and Eaton, W. A. (1985) Nanosecond optical spectra of iron−cobalt hybrid hemoglobins: geminate recombination, conformational changes, and intersubunit communication, *Biochemistry 24*, 2667−2679.

15. Dickerson, R. E., and Geis, I. (1983) *Hemoglobin: Structure, Function, Evolution, and Pathology*, Benjamin/Cummings, Menlo Park.

16. Smith, F. R., and Ackers, G. K. (1985) Experimental resolution of cooperative free energies for the ten ligation states of human hemoglobin, *Proc. Natl. Acad. Sci. U.S.A. 82*, 5347−5351.

17. Perrella, M., Benazzi, L., Shea, M. A., and Ackers, G. K. (1990) Subunit hybridization studies of partially ligated cyanomethemoglobins using a cryogenic method. Evidence for three allosteric states, *Biophys. Chem. 35*, 97−103.

18. Ackers, G. K. (1990) The energetics of ligand-linked subunit assembly in hemoglobin require a third allosteric structure, *Biophys. Chem. 37*, 371−382.

19. Speros, P. C., LiCata, V. J., Yonetani, T., and Ackers, G. K. (1991) Experimental resolution of cooperative free energies for the 10 ligation species of cobalt(II)/iron(II)-CO hemoglobin, *Biochemistry 30*, 7254−7262.

20. Daugherty, M. A., Shea, M. A., and Ackers, G. K. (1994) Bohr effects of the partially ligated (CN-met) intermediates of hemoglobin as probed by quaternary assembly, *Biochemistry 33*, 10345−10357.

21. Huang, Y., and Ackers, G. K. (1995) Enthalpic and entropic components of cooperativity for the partially ligated intermediates of hemoglobin support a mechanism, *Biochemistry 34*, 6316−6327.

22. Huang, Y., Doyle, M. L., and Ackers, G. K. (1996) The oxygen-binding intermediates of human hemoglobin: evaluation of their contributions to cooperativity using zinc-containing hybrids, *Biophys. J. 71*, 2094−2105.

23. Ackers, G. K., Holt, J. M., Huang, Y., Grinkova, Y., Klinger, A. L., and Denislov, I. (2000) Confirmation of a unique intra-dimer cooperativity in the human hemoglobin α₁β₁ half-oxygenated

24. intermediate supports the symmetry rule model of allosteric regulation, *Proteins Suppl. 4*, 23−43.

25. Imai, K., Yonetani, T., and Ikeda-Saito, M. (1977) Allosteric effects in cobaltohemoglobin as studied by precise oxygen equilibrium measurements, *J. Mol. Biol. 109*, 83−97.

26. Fermi, G., Perutz, M. F., Dickinson, L. C., and Chien, J. C. W. (1982) Structure of human deoxy cobalt hemoglobin, *J. Mol. Biol. 155*, 495−505.

27. Fujii, M., Hori, H., Miyazaki, G. Morimoto, H., and Yonetani, T. (1993) The porphyrin-iron hybrid hemoglobins: Absence of the Fe−His bonds in one type of subunits favors a deoxy-like structure with low oxygen affinity, *J. Biol. Chem. 268*, 15386−15393.

28. Shulman, R. G., Hopfield, J. J. and Ogawa, S. (1975) Allosteric interpretation of hemoglobin properties, *Q. Rev. Biophys. 8*, 325−420.

29. Shulman, R. G., Ogawa, S. and Mayer, A. (1982) The Two-State Model of Hemoglobin: Hb Kansas as a Model for the Low-Affinity State, in *Hemoglobin and Oxygen Binding* (Ho, C., et al., Eds.) pp 205−209, Elsevier, New York.

30. Koshland, D. E., Nemethy, G., and Filmer, D. (1966) Comparison of experimental binding data and theoretical models in proteins containing subunits, *Biochemistry 5*, 365−385.

31. Perutz, M. F. (1970) Stereochemistry of cooperative effects in haemoglobin, *Nature 228*, 726−739.

32. Szabo, A., and Karplus, M. (1972) A mathematical model for structure−function relations in hemoglobin, *J. Mol. Biol. 72*, 163−197.

33. Herzfeld, J., and Stanley, H. E. (1974) A general approach to cooperativity and its application to the oxygen equilibrium of hemoglobin and its effectors, *J. Mol. Biol. 82*, 231−265.

34. Lee, A., and Karplus, M. (1983) Structure-specific model of hemoglobin cooperativity, *Proc. Natl. Acad. Sci. U.S.A. 80*, 7055−7059.

35. Perutz, M. F., Fermi, G., Luisi, B., Shaanan, B., and Liddington, R. C. (1987) Stereochemistry of cooperative mechanisms in hemoglobin, *Acc. Chem. Res. 20*, 309−321.

36. Brzozowski, A., Derewenda, Z., Dodson, E., Dodson, G., Grabowski, M., Liddington, R., Skarzynski, T., and Vallely, D. (1984) Bonding of molecular oxygen to T state human haemoglobin, *Nature 307*, 74−76.

37. Mozzarelli, A, Rivetti, C., Rossi, G. L., Henry, E. R., and Eaton, W. A. (1991) Crystals of haemoglobin with the T quaternary structure bind oxygen noncooperatively with no Bohr effect, *Nature 351*, 416−419.

38. Rivetti, C., Mozzarelli, A., Rossi, G. L., Henry, E. R., and Eaton, W. A. (1993) Oxygen binding by single crystals of hemoglobin, *Biochemistry 32*, 2888−2906.

39. Shibayama, N., and Saigo, S. (1995) Fixation of the quaternary structures of human adult haemoglobin by encapsulation in transparent porous silica gels, *J. Mol. Biol. 251*, 203−209.

40. Sawicki, C. A., and Gibson, Q. H. (1976) Quaternary conformational changes in human hemoglobin studied by laser photolysis of carboxyhemoglobin, *J. Biol. Chem. 251*, 1533−1542.